

# FDSG: Forecasting Dynamic Scene Graphs

Yi Yang      Yuren Cong  
TNT, Leibniz University Hannover  
yangyi, cong@tnt.uni-hannover.de

Bodo Rosenhahn  
TNT, Leibniz University Hannover  
rosenhahn@tnt.uni-hannover.de

Hao Cheng  
ITC, University of Twente  
h.cheng-2@utwente.nl

Michael Ying Yang  
Visual Computing Group, University of Bath  
myy35@bath.ac.uk

## Abstract

*Dynamic scene graph generation extends scene graph generation from images to videos by modeling entity relationships and their temporal evolution. However, existing methods either generate scene graphs from observed frames without explicitly modeling temporal dynamics, or predict only relationships while assuming static entity labels and locations. These limitations hinder effective extrapolation of both entity and relationship dynamics, restricting video scene understanding. We propose Forecasting Dynamic Scene Graphs (FDSG), a novel framework that predicts future entity labels, bounding boxes, and relationships, for unobserved frames, while also generating scene graphs for observed frames. Our scene graph forecast module leverages query decomposition and neural stochastic differential equations to model entity and relationship dynamics. A temporal aggregation module further refines predictions by integrating forecasted and observed information via cross-attention. To benchmark FDSG, we introduce Scene Graph Forecasting, a new task for full future scene graph prediction. Experiments on Action Genome show that FDSG outperforms state-of-the-art methods on dynamic scene graph generation, scene graph anticipation, and scene graph forecasting. Codes will be released upon publication.*

## 1. Introduction

Dynamic Scene Graph Generation (DSGG) is a critical task in visual understanding that extends scene graph generation [18] from images to videos. Unlike static scene graph generation of *triplets*  $\langle \text{subject-predicate-object} \rangle$  in a single image, DSGG requires modeling dynamic interactions over time, leveraging both spatial and temporal dependencies. This enables a more comprehensive representation of scenes, crucial for applications such as action recognition [21], video analysis [7, 32], and surveillance [6].

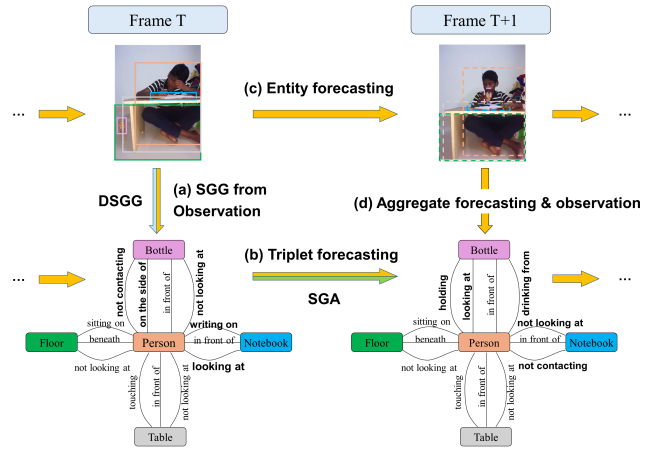


Figure 1. Comparison between existing tasks and our FDSG framework. (a) DSGG generates scene graphs and entity bounding boxes from observed video. (b) SGA predicts scene graphs without bounding boxes for future unobserved video. In contrast, FDSG forecasts both scene graph (b) and predicts entity labels and bounding boxes (c) in the future, while also aggregating observed-frame information to enhance both generation and forecasting (d). Our FDSG employs a one-stage end-to-end design, without explicit object tracking, and incorporates forecasting error as an auxiliary loss, enabling joint learning of DSGG and SGA.

Most existing methods [9, 17, 40–42, 48] employ an interpolation strategy, meaning that the target frame and reference frames need to be observed in order to generate a scene graph for the target frame, as illustrated in Fig. 1(a). Although these methods effectively generate scene graphs for individual frames, they lack a learning strategy to forecast the temporal dynamics and continuity across frames, preventing them from extrapolating temporal dependencies to enhance scene graph generation in videos.

In contrast, extrapolation scene graph generation goes beyond the current frames by forecasting the evolving relationships between entities in future frames based on observed frames. This forecasting-driven approach has

demonstrated clear advantages in text and video generation [28] and language modeling [4], where training models to predict future content encourages the development of richer, more generalizable representations. Despite this, only a couple of methods have explored forecasting for DSGG. Notable examples include APT [24], which leverages pre-training to learn temporal correlations of visual relationships across frames, and SceneSayer [33], which introduces the task of Scene Graph Anticipation (SGA) of predicting future object interactions, as shown in Fig. 1(b). However, both methods adopt a narrow form of extrapolation, focusing almost exclusively on relationships while making the overly rigid assumption that entity labels and locations remain static. This oversimplification significantly limits their ability to handle realistic dynamic scenes, where entities often undergo substantial changes in both appearance and position – such as a bottle being picked up and moved by a person, as illustrated in Fig. 1. Moreover, effectively fusing predicted information with observed frames remains an open challenge. This fusion is crucial for accurate temporal modeling but has been largely overlooked in existing extrapolation-based methods for dynamic scene graph generation, limiting their ability to understand complex scenes.

To address these limitations, we introduce **Forecasting Dynamic Scene Graphs**, termed **FDSG**. It fully embraces extrapolation by forecasting future relationships, entity labels, and bounding boxes (Fig. 1(b),(c)). The predicted information is further incorporated with the observation at the current frame (Fig. 1(d)), fostering a more comprehensive understanding in videos. Specifically, a novel Forecast Module uses the query decomposition formulation in DINO [46], a state-of-the-art object detection model, to explicitly model entity label and location dynamics, and Neural Stochastic Differential Equations (NeuralSDE) [20, 33] to holistically model the time evolution of triplets from a continuous-time perspective. The temporal aggregation module then uses cross-attention mechanisms to incorporate the forecasted scene graph representations with the high-confidence observed information selectively, enhancing the generated scene graph for the target frame.

Overall, our **key contributions** are as follows:

- We propose Scene Graph Forecasting (SGF), a new task that forecasts complete future scene graphs – including entities, bounding boxes, and interactions – from a video stream. This new task complements the existing DSGG and SGA tasks, providing a comprehensive evaluation for extrapolation-based scene graph generation.
- We propose Forecasting Dynamic Scene Graphs (FDSG), a novel framework for simultaneous scene graph generation and forecasting, as illustrated in Fig. 2. FDSG includes a Forecast Module to handle forecasting challenges and an effective Temporal Aggregation Module to enhance DSGG using SGF results, and vice versa.

- We rigorously validate our proposed model with the Action Genome dataset [16] on DSGG, SGA, and SGF tasks. Our method achieves superior performance on the SGF task and outperforms the existing methods on both DSGG and SGA tasks, demonstrating that learning to extrapolate can benefit the model’s overall ability of dynamic scene understanding.

## 2. Related Work

**Dynamic Scene Graph Generation.** The Dynamic Scene Graph Generation (DSGG) task aims to generate a scene graph for each video frame, focusing on modeling the temporal dynamics of entities and their pairwise relationships. Early static [26, 27, 39, 43, 45] and dynamic scene graph generation [9, 17, 40, 42] models rely on off-the-shelf object detectors such as Faster-RCNN [34], which are also known as two-stage methods. Once entity representations from each frame are obtained, these two-stage methods typically utilize dedicated self-attention [9] or cross-attention layers [17, 40, 42] for temporal feature aggregation. With the recent success of the Transformer-based object detection model DETR [2], more attention has been paid to DETR-based one-stage scene graph generation for images [10, 15, 23] and videos [41, 48]. These methods use a fixed set of queries for entity detection, facilitating finding the correspondence between the target and reference entities or triplets. These methods, although having achieved remarkable success in benchmark datasets, they utilize both the target frame and the reference frames to interpolate scene graphs from observed data. As a result, these models lack the capacity to predict future video frames accurately enough to support dynamic scene graph forecasting.

**Anticipating Visual Relationships.** Modeling relationships dynamics across frames in scene graphs is crucial for DSGG. The first exploration of anticipating future visual relationships comes from APT [24], which introduces anticipatory pertaining to predict predicates (relationships) in the next frame using reference frames, then fine-tuned on all frames. While this improves the performance on DSGG, APT relies on conventional metrics and does not explicitly evaluate anticipation. More recently, Peddi *et al.* [33] formalized a Scene Graph Anticipation (SGA) task with a prediction model called SceneSayer, which combines two-stage DSGG models STTran [9] and DSG-DETR [11] and adopts a Neural Differential Equation-based dynamics model to predict future relationships. It focuses on the correctness of predicted visual relationships in the scene graph, assuming that the entity labels and locations remain unchanged in the future. The new evaluation metrics in SGA focus solely on predicting correct relationships, assuming fixed entity labels and locations. However, this overlooks entity dynamics, limiting anticipatory capability to predicting relationships under rigid location and label constraints.

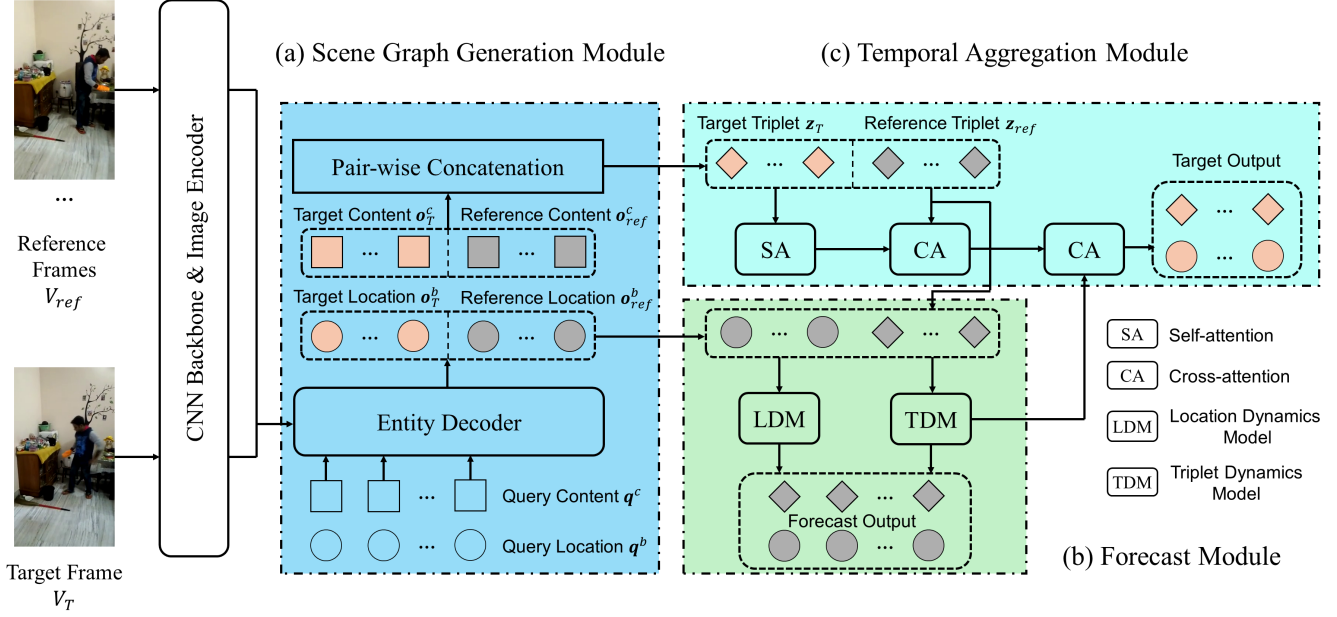


Figure 2. Our FDSG Framework carries out Dynamic Scene Graph Generation (DSGG) and Scene Graph Forecasting (SGF) simultaneously to fully exploit temporal dependencies. Video features are extracted using a CNN backbone and a DINO encoder. Then, **(a)** Scene Graph Generation Module generates scene graph representations for each observed frame. Subsequently, **(b)** Forecast Module forecasts a scene graph from a reference frame to the target frame. Finally, **(c)** Temporal Aggregation Module aggregates information from DSGG and SGF to jointly enhance model performance.

Unlike the above methods with partial forecasting, our proposed Scene Graph Forecasting (SGF) task extends the relationship prediction to include both entity locations and labels. This allows for a more comprehensive modeling of motion and relationship dynamics across frames. Moreover, we adopt a one-stage end-to-end method to achieve DSGG and SGF simultaneously with mutual benefits.

**Anticipating Entity Labels and Locations.** Anticipating entity labels and locations have been explored in various domains. For example, Object Forecasting [19, 37] aims to predict future bounding boxes of tracked objects, which is closely related to object tracking [1]. [19, 37] use RNNs to model entity evolution which rely heavily on tracked object trajectory and low-level features from optical flow estimation [44], but ignore information from high-level scene understanding, such as object interactions. Action Anticipation, on the other hand, aims to predict what is going to happen in the scene given a portion of the activity video [12, 13, 31, 35]. It requires video understanding from an overview perspective. Recently, a novel task, known as Future Action Localization [8], aims to predict the bounding boxes for the central action-taking person(s) in videos from a third-person view. The proposed model AdamsFormer [8] models the dynamics of the central person using a Neural Ordinary Differential Equation model [5] with features extracted from a CNN-based video encoder. However, this task overlooks modeling other objects interacting with the central person. In comparison, our proposed method for

forecasting dynamic scene graphs takes a more comprehensive perspective, which includes anticipating relationships of interactions between various entities, entity labels, and locations. This forecasting process requires modeling both low-level features for entity prediction and localization, and high-level understanding of interaction dynamics between entities within the scene.

### 3. Method

#### 3.1. Problem Formulation

A scene graph is a structured representation of visual relationships in a given scene, with nodes representing object instances and edges representing pairwise instance relationships. Formally, in frame  $t$ , each node  $o_t(k_t)$  is defined by its category  $c_t(k_t) \in \mathcal{C}$ , where  $\mathcal{C}$  is the object category set and  $k_t \in [1, K_t]$  with  $K_t$  being the number of objects.  $b_t(k_t) \in [0, 1]^4$  denotes the corresponding normalized box with center coordinates and width and height. Each edge represents a relationship  $p_t(i, j) \in \mathcal{P}$  between two objects  $o_t(i)$  and  $o_t(j)$ , where  $\mathcal{P}$  is the set of predicates. If it is not otherwise specified, we use  $i$  to refer to a *subject* entity and  $j$  to an *object* entity, in order to differentiate the direction of a *predicate* from the subject to the object. Together, a triplet is denoted as  $r_t(i, j) = (o_t(i), p_t(i, j), o_t(j))$  and the scene graph for frame  $t$  is denoted as  $G_t = \{r_t(i, j)\}_{ij}$ . Given an input video  $V_{t=1}^H = \{V_t\}$ , where  $t \in \{1, \dots, T, T+1, \dots, H\}$ , we

introduce the following tasks:

**Dynamic Scene Graph Generation (DSGG):** with all frames being observed, the model outputs a scene graph for every frame:  $\{\hat{G}_t\}_{t=1}^H$ ;

**Scene Graph Anticipation (SGA):** with frames up to a specific time stamp  $T$  being observed, the model predicts *un-localized* future scene graphs:  $\{\hat{G}_t\}_{t=T+1}^H$ . Entities in the anticipatory time horizon ( $t \in \{T+1, \dots, H\}$ ) are assumed to be the same as last observed in frame  $T$  with no bounding boxes anticipation [33];

**Scene Graph Forecasting (SGF):** with the same observation time horizon as SGA, but the model predicts both the evolution of predicates and future entity labels and bounding boxes in the anticipatory time horizon. The task of SGF is illustrated in Fig.3.

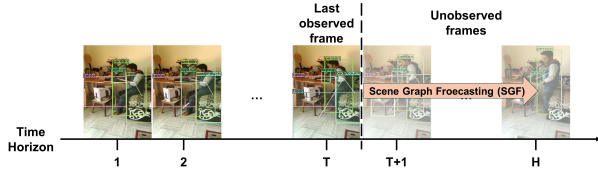


Figure 3. Illustration of the proposed SGF task.

### 3.2. Overview

The overall workflow of our proposed method is illustrated in Fig. 2. Our *Scene Graph Generation Module* (Fig. 2(a)) generates static scene graphs for each input frame. The *Forecast Module* (Fig. 2(b)) forecasts scene graphs in the future. The *Temporal Aggregation Module* (Fig. 2(c)) aggregates temporal information from observed video and from scene graph forecasts, and updates the final prediction for the target frame.

### 3.3. Scene Graph Generation Module

The Scene Graph Generation Module employs DINO [46] to detect all entities  $\{o_t(k)\}_{k=1}^{K_t}$  in each input frame  $V_t$ . DINO consists of a backbone, a multi-layer Transformer encoder, and a multi-layer Transformer decoder. It uses a fixed set of  $N_q$  queries  $\mathbf{q} = \{q_0, q_1, \dots, q_{N_q}\}$  for entity detection. Each query  $q = \{q^c, q^b\}$  is composed of content  $q^c$  and location  $q^b$ . Accordingly, DINO outputs decomposed representations for detected entities:  $\hat{o} = \{\hat{o}^c, \hat{o}^b\}$ . Note that for brevity here, we omit the denoising branch in DINO.

To form triplet representations  $z(i, j)$ , we follow common practice in the literature [9, 15, 33] and concatenate the output content representation  $\hat{o}^c(i)$  of the subject with the content representation  $\hat{o}^c(j)$  of all other objects. The predicate is implicitly encoded:

$$z(i, j) = [\hat{o}^c(i); \hat{o}^c(j)], \quad (1)$$

where  $[\cdot; \cdot]$  denotes the concatenation operation.

Finally, the scene graph classification head includes a linear layer to classify entity labels, a three-layer Multi-Layer Perceptron (MLP) for bounding box regression, and a two-layer MLP for predicate classification.

### 3.4. Forecast Module

Our Forecast Module consists of a Triplet Dynamics Model and a Location Dynamics Model (LDM). In the Triplet Dynamics Model, we utilize a NeuralSDE (see Supplementary B.3 for more details) to forecast triplet representations from state  $z_{T_0}$ , where  $T_0 \in \{1, \dots, T\}$ , to state  $z_{T_0+\Delta T}$  at  $\Delta T$  time steps later, inspired by SceneSayer [33]:

$$z_{T_0+\Delta T} = \text{NeuralSDE}(z_{T_0}, \Delta T). \quad (2)$$

To obtain forecasts for entity contents, we reverse the concatenation operation in Eq. (1) and split the forecasted triplet representation:

$$[\hat{o}_{T_0+\Delta T}^c(i); \hat{o}_{T_0+\Delta T}^c(j)] = z_{T_0+\Delta T}(i, j). \quad (3)$$

Our LDM predicts entity location representations:

$$\hat{o}_{T_0+\Delta T}^b(j) = \text{LDM}(\hat{o}_{T_0}^b, \Delta T). \quad (4)$$

While intuitively, another NeuralSDE can be adopted for the LDM, in our experiments, we found that the LDM can be reduced to an elegantly effective Identity Mapping. More detailed ablation study on this can be found in Table 5.

The classification head for forecasted scene graphs takes the same form as in the Scene Graph Generation module:

$$\hat{c}_{T_0+\Delta T}(j) = \text{Linear}(\hat{o}_{T_0+\Delta T}^c(j)), \quad (5)$$

$$\hat{b}_{T_0+\Delta T}(j) = \sigma(\text{MLP}(\hat{o}_{T_0+\Delta T}^c(j)) + \sigma^{-1}(\hat{o}_{T_0+\Delta T}^b(j))), \quad (6)$$

$$\hat{p}_{T_0+\Delta T}(i, j) = \text{MLP}(z_{T_0+\Delta T}(i, j)), \quad (7)$$

where  $\sigma$  denotes the sigmoid function and  $\sigma^{-1}$  is its inverse.

In the case where the LDM is an Identity Mapping,  $\hat{o}_{T_0+\Delta T}^b = \hat{o}_{T_0}^b$ , and Eq. (6) reduces to

$$\hat{b}_{T_0+\Delta T} = \sigma(\text{MLP}(\hat{o}_{T_0+\Delta T}^c + \sigma^{-1}(\hat{o}_{T_0}^b))). \quad (8)$$

This means that the anticipated object bounding box  $\hat{o}_{T_0+\Delta T}^b$  is the sum of a reference bounding box from the last observation  $\hat{o}_{T_0}^b$ , and a residual term provided by the anticipated object content representation  $\text{MLP}(\hat{o}_{T_0+\Delta T}^c(j))$ . The Triplet Dynamics Model in Eq. (2) is therefore responsible for learning such a residual. More details and analysis on the realization of the LDM are presented in Sec. 4.3.

### 3.5. Temporal Aggregation Module

For each frame  $V_t$ , SGG Module generates a set of triplet representations  $Z_t = \{z_t(i, j) \mid i \in \text{obj}, j \in \text{obj}\}$ . To aggregate temporal information for the target frame  $V_{T_g}$ , following [41, 49], we sample reference frames  $\{V_{\text{ref}_1}, \dots, V_{\text{ref}_n}\}$



from the video. Then we use cascaded Transformer decoders to aggregate information, first from the reference triplet representations  $Z_{\text{ref}} = \{Z_{\text{ref}_1}, \dots, Z_{\text{ref}_n}\}$ , and then from forecasted representations  $Z_{T_0+\Delta T}$ .

For reference frame aggregation, the triplet representations of the target frame  $Z_{T_g}$  is updated by first doing self-attention and then cross-attention with reference triplets:

$$Z_{T_g} = \text{CrossAttn}(\text{SelfAttn}(Z_{T_g}), \text{TopK}(Z_{\text{ref}}, k)) \quad (9)$$

where TopK selects  $k$  most confident reference triplets in terms of object and predicate classification scores. We use multiple decoders and the value of  $k$  is gradually reduced in order to obtain progressively refined features. See Supplementary B.1 for details on attention layers.

To aggregate information from forecasts, we use

$$Z_{T_g} = \text{CrossAttn}(\text{SelfAttn}(Z_{T_g}), Z_{T_0+\Delta T}). \quad (10)$$

where  $T_0$  is selected from a reference frame  $\text{ref}_n$  and  $T_0 + \Delta T = T_g$ . As shown in [8, 33], a larger anticipatory window benefits NeuralSDE performance; hence, we select  $\text{ref}_n$  such that the time difference  $\Delta T$  is as large as possible. A more detailed analysis can be found in [33].

We first aggregate information from reference frames with lower uncertainty, followed by forecasts with higher uncertainty. Alternative aggregation strategies underperform, and details are provided in Supplementary C.4.

### 3.6. Training and Inference

**Training.** Our model simultaneously outputs DSGG and SGF results, and the loss function has two components:

$$\mathcal{L} = \sum_{t=1}^H (\mathcal{L}_t^{\text{DSGG}} + \mathcal{L}_t^{\text{SGF}}) \quad (11)$$

For each frame  $V_t$ , a fixed set of triplets  $\{\hat{r}_t(k)\}_{k=1}^{N_r}$  is predicted by the Scene Graph Generation Module, where  $N_r$  denotes the total number of triplets derived from the fixed set of predicted entities  $\hat{o}_t = \{\hat{o}_t(i)\}_{i=1}^{N_q}$ . We use the Hungarian algorithm as in DETR [2] to find the optimal one-to-one matching  $\hat{\rho} \in P$  between the prediction set  $\hat{G}_t = \{\hat{r}_t(k)\}_{k=1}^{N_r}$  and the ground truth set  $G_t = \{r_t(k)\}_{k=1}^{N_r}$ , where  $G_t$  is padded with  $\emptyset$  to the same length as  $\hat{G}_t$ . The optimal matching  $\hat{\rho}$  is found by

$$\hat{\rho} = \arg \min_{\rho \in P} \sum_{k=1}^{N_r} \mathcal{L}_{\text{match}}(r(k), \hat{r}(\rho(k))) \quad (12)$$

where  $\mathcal{L}_{\text{match}}(r(k), \hat{r}(\rho(k)))$  is the matching loss to assign predicted triplet  $\hat{r}$  with index  $\rho(i)$  to ground truth triplet  $r(i)$ . This matching loss is a sum of entity classification

loss, predicate classification loss and entity bounding box regression loss:

$$\mathcal{L}_{\text{match}}(r(k), \hat{r}(\rho(k))) = \sum_{l \in \{s, o, p\}} \alpha_l \mathcal{L}_{\text{cls}}^l + \sum_{l \in \{s, o\}} \beta_l \mathcal{L}_{\text{box}}^l \quad (13)$$

where  $\{s, o, p\}$  denotes subject, object, predicate respectively, and  $\alpha_l$  and  $\beta_l$  are weighting factors. We use focal loss [36] for classification  $\mathcal{L}_{\text{cls}}$ , and a weighted sum of L1-loss and GIoU-loss for bounding box regression  $\mathcal{L}_{\text{box}}$ . When calculating the predicate classification loss, we follow OED [41] and ignore the loss between the prediction and any padded ground truth.

We use the same Hungarian Matching loss for SGF. During training, the model only outputs forecasted triplets for the target frame. We select a reference frame and use it to forecast the scene graph for the target frame, as specified in Eq. (10). Therefore, both the Scene Graph Generation Module and the Scene Graph Forecast Module output predictions for the same target frame. Unlike SGA, we do not need to store additional samples or labels for multiple observed and anticipatory targets.

**Inference.** For DSGG, our model sees the entire video  $V^H$  and samples  $n$  reference frames  $\{V_{\text{ref}_1}, \dots, V_{\text{ref}_n}\}$ . Our model input is therefore  $\{V_{\text{ref}_1}, \dots, V_{\text{ref}_n}\}$  and the target frame  $V_{T_g}$ , and the output is the scene graph  $\hat{G}_{T_g}$ .

For SGA and SGF, our model only sees part of the video  $\{V_1, \dots, V_T\}$  and samples  $n$  reference frames  $\{V_{\text{ref}_1}, \dots, V_{\text{ref}_n}\}$  from the observed part. Our model inputs in this case are  $\{V_{\text{ref}_1}, \dots, V_{\text{ref}_n}\}$  and the last observed frame  $V_T$ . Our model generates a scene graph  $\hat{G}_T$  for the last observed frame, and from  $\hat{G}_T$  it forecasts scene graphs  $\{\hat{G}_t\}_{t=T+1}^H$  for a future time window of length  $H - T$ .

## 4. Experiments

### 4.1. Experimental Settings

**Dataset.** We evaluate the proposed model on the Action Genome dataset [16], which offers frame-level annotations for dynamic scene graph generation tasks. It encompasses 234,253 frames with 476,229 bounding boxes representing 35 object classes (excluding “person”) and 1,715,568 instances across 25 relationship (predicate) classes. These relationships are categorized into three types: attentional (e.g., a person looking at an object), spatial (e.g., object positions relative to each other), and contacting (e.g., interactions such as holding or eating). Notably, this dataset supports multi-label annotations, with 135,484 subject-object pairs annotated with multiple spatial or contact relationships, facilitating nuanced analysis of complex human-object interactions. This allows us to follow the two widely recognized strategies [3, 22] to build scene graphs and evaluate their performance: (1) *With Constraint*: enforcing a

Table 1. Comparison with state-of-the-art Dynamic Scene Graph Generation (DSGG) methods on Action Genome for Scene Graph Detection (SGDET). Best values are highlighted in **boldface**.

SGDET, $IoU \geq 0.5$	Recall@K (R@K) $\uparrow$						Mean Recall@K (mR@K) $\uparrow$					
	With Constraint			No Constraint			With Constraint			No Constraint		
Method	10	20	50	10	20	50	10	20	50	10	20	50
RelDN [47]	9.1	9.1	9.1	13.6	23.0	36.6	3.3	3.3	3.3	7.5	18.8	33.7
VCtree [38]	24.4	32.6	34.7	23.9	35.3	46.8	-	-	-	-	-	-
TRACE [40]	13.9	14.5	14.5	26.5	35.6	45.3	8.2	8.2	8.2	22.8	31.3	41.8
GPS-Net [26]	24.7	33.1	35.1	24.4	35.7	47.3	-	-	-	-	-	-
STTran [9]	25.2	34.1	37.0	24.6	36.2	48.8	16.6	20.8	22.2	20.9	29.7	39.2
APT [24]	26.3	36.1	38.3	25.7	37.9	50.1	-	-	-	-	-	-
DSG-DETR [11]	30.4	34.9	36.0	32.3	40.9	48.2	18.0	21.3	22.0	23.6	30.1	36.5
TEMPURA [30]	28.1	33.4	34.9	29.8	38.1	46.4	18.5	22.6	23.7	24.7	33.9	43.7
OED [41]	33.5	40.9	48.9	35.3	44.0	51.8	20.9	26.9	32.9	26.3	39.5	49.5
Ours	<b>35.3</b>	<b>42.9</b>	<b>49.8</b>	<b>37.2</b>	<b>47.2</b>	<b>56.5</b>	<b>22.2</b>	<b>27.8</b>	<b>33.0</b>	<b>27.8</b>	<b>42.0</b>	<b>54.1</b>

Table 2. Comparison with state-of-the-art Scene Graph Anticipation (SGA) methods in the Action Genome Scenes (AGS). Best values are highlighted in **boldface**.

AGS, $\mathcal{F} = 0.5, IoU \geq 0$	Recall@K (R@K) $\uparrow$						Mean Recall@K (mR@K) $\uparrow$					
	With Constraint			No Constraint			With Constraint			No Constraint		
Method	10	20	50	10	20	50	10	20	50	10	20	50
STTran++ [9, 33]	19.7	30.2	31.8	16.6	29.1	51.5	6.3	11.3	12.3	6.6	14.7	33.4
DSG-DETR++ [11, 33]	20.7	30.3	31.6	17.4	30.5	51.9	6.4	11.0	11.7	8.4	17.0	33.9
SceneSayerODE [33]	25.9	32.6	34.8	26.4	36.6	49.8	11.6	15.2	16.4	14.3	21.4	36.0
SceneSayerSDE [33]	27.3	34.8	37.0	28.4	38.6	51.4	12.4	16.6	18.0	16.3	25.1	39.9
Ours	<b>28.3</b>	<b>36.5</b>	<b>45.3</b>	<b>30.1</b>	<b>40.4</b>	<b>52.2</b>	<b>18.1</b>	<b>23.5</b>	<b>27.5</b>	<b>23.2</b>	<b>34.3</b>	<b>45.8</b>

unique interaction for each pair. (2) *No Constraint*: allowing multiple relationships between the same pair.

**Evaluation Metrics.** We adopt the standard metrics *Recall@K (R@K)* and *mean Recall@K (mR@K)* to evaluate our model’s performance under both *With Constraint* and *No Constraint* strategies, where higher values indicate better coverage of true relationships. Following previous works, we set  $K \in \{10, 20, 50\}$ . For DSGG and SGF, we primarily evaluate our model using the most challenging protocol, Scene Graph Detection (SGDET), which requires predicting entity labels, bounding boxes, and pairwise relationships for a target frame. A predicted entity bounding box is considered correct if its Intersection over Union (IoU) with the ground truth box exceeds 0.5. Additional details on DSGG evaluation protocols Scene Graph Classification (SGCLS) and Predicate Classification (PredCLS) are provided in the Supplementary Materials. For SGA and SGF, to split the observation and forecasting time horizons, we use  $\mathcal{F}$ , the fraction of observed frames within the total video frames. A typical value is  $\mathcal{F} = 0.5$ , meaning the first half of the video is observed, while the second half is used for evaluation. For SGA, our model is evaluated on Action Genome Scenes, Partially Grounded Action Genome Scenes, and Grounded Action Genome Scenes, following

[33]. Notably, in SGA, bounding box is not evaluated [33], therefore we use an IoU threshold of 0.

**Implementation Details.** Our model is initialized with 4-scale DINO pretrained for 36 epochs on the COCO 2017 Object Detection Dataset [25], which consists of 6 Transformer layers for encoder and decoder respectively, and uses ResNet50 [14] as the backbone. The number of entity queries is set to 100. Following OED [41], we set  $\text{TopK} = \{80n, 50n, 30n\}$ , where  $n = 2$ , denoting the number of reference frames. For the NeuralSDE in our Triplet Dynamics Model, we employ a solver with a reversible Heun method, the same as in SceneSayer [33].  $\mathcal{F}$  is set to  $\{0.3, 0.5, 0.7, 0.9\}$ . More details of our model training are provided in Supplementary B.4.

## 4.2. Quantitative Results and Comparison

**Dynamic Scene Graph Generation.** We evaluate our method on DSGG using the SGDET protocol, with results summarized in Table 1. Our approach consistently outperforms state-of-the-art methods across all metrics in both *With Constraint* and *No Constraint* settings, in particular achieving a notable performance gain over OED [41] in both R@50 and mR@50. For comparison in the PredCLS and SGCLS tasks, please refer to Supplementary C.1.

Table 3. The performance of Scene Graph Forecasting (SGF) on Action Genome for Scene Graph Detection (SGDET). Best values are highlighted in **boldface**.

SGDET, $\mathcal{F} = 0.5$ $IoU \geq 0.5$	Recall@K (R@K) $\uparrow$						Mean Recall@K (mR@K) $\uparrow$					
	With Constraint			No Constraint			With Constraint			No Constraint		
Method	10	20	50	10	20	50	10	20	50	10	20	50
SceneSayerODE+ [33]	0.9	1.0	1.1	0.9	1.2	1.6	0.5	0.6	0.6	0.6	1.0	1.7
SceneSayerSDE+ [33]	2.5	3.2	3.4	2.6	3.7	5.0	1.1	1.6	1.7	1.4	2.2	4.4
Ours	<b>10.6</b>	<b>13.3</b>	<b>15.5</b>	<b>12.0</b>	<b>15.5</b>	<b>18.8</b>	<b>8.4</b>	<b>11.2</b>	<b>12.6</b>	<b>11.4</b>	<b>17.2</b>	<b>22.5</b>

**Scene Graph Anticipation.** Table 2 presents our results on SGA with an observation fraction of  $\mathcal{F} = 0.5$  on Action Genome Scenes. Our method outperforms SceneSayer [33] across all metrics, achieving up to 50% improvement in mR@10 and mR@50, and averaging a 40% gain across Mean Recall metrics, highlighting our model’s effectiveness in reducing prediction bias. Additional results for  $\mathcal{F} = 0.3, 0.7, 0.9$  and for Grounded / Partially Grounded protocols are provided in Supplementary C.2.

**Scene Graph Forecasting.** We report our SGF results at  $\mathcal{F} = 0.5$  in Table 3. Baselines are adapted from SceneSayerODE/SDE [33], where predicted predicate representations are fed into MLPs for bounding box forecasting (see Supplementary B.5 for details). While these models perform well for predicate anticipation, they show limited capacity for entity forecasting. In contrast, our model significantly outperforms them, demonstrating a stronger ability to learn temporal dynamics. Together with our improvements in DSGG and SGA (Tables 1, 2), this highlights the advantages of our forecasting-driven design.

**Entity Forecasting in SGF.** We explicitly evaluate entity forecasting using Object Detection Recall. At  $\mathcal{F} = 0.5$  and  $IoU \geq 0.5$ , FDSG achieves a recall of 43.85, significantly outperforming a baseline recall of 40.33 that reuses entities from the last observed frame. See Supplementary C.3 for detailed evaluation with different  $\mathcal{F}$  and IoU thresholds.

### 4.3. Ablation Studies

**Module effectiveness.** We assess the contribution of each component in our model, with results shown in Table 4. The baseline model (#1) uses only spatial modeling (S), without explicit temporal modeling. Adding the Temporal Aggregation Module (T) in model (#2) yields a clear performance boost, surpassing OED. Incorporating the Triplet Dynamics Model (TDM) in model (#3) enables SGA and further improves DSGG, demonstrating the benefits of learning to forecast. Enabling the Location Dynamics Model (LDM) in model (#6) extends capability to SGF, while also enhancing both SGA and DSGG. When the Temporal Aggregation Module is removed (models #4 and #5), DSGG performance drops to baseline levels, and both SGA and SGF are negatively impacted. This highlights the importance of temporal aggregation in learning rich representations for both predic-

tion and forecasting. Model (#4) achieves a higher R@20 on SGA than the full model (#6), but shows a significant drop in mR@20, indicating reduced robustness. Further analysis is provided in Supplementary C.3.

Table 4. Ablation study of model components. S - Scene Graph Generation Module; T - Temporal Aggregation Module, TDM - Triplet Dynamics Model; LDM - Location Dynamics Model; DSGG - Dynamic Scene Graph Generation; SGA - Scene Graph Anticipation; SGF - Scene Graph Forecasting. Best and second best values are in **boldface** and underlined, respectively.

#	Model Component				SGDET / AGS, $\mathcal{F} = 0.5$ With Constraint R@20 $\uparrow$		
	S	T	TDM	LDM	DSGG	SGA	SGF
1	✓				41.0	-	-
2	✓	✓			42.2	-	-
3	✓	✓	✓		<u>42.4</u>	36.3	-
4	✓		✓		41.0	<b>36.8</b>	-
5	✓		✓	✓	40.8	35.1	<u>12.2</u>
6	✓	✓	✓	✓	<b>42.9</b>	<u>36.5</u>	<b>13.3</b>

Table 5. Comparison of different realizations for a Location Dynamics Model (LDM). IM denotes the Identity Mapping.

Task	LDM	SGDET / AGS, $\mathcal{F} = 0.5$ With Constraint $\uparrow$		
		R@10	R@20	R@50
DSGG	IM	<u>35.3</u>	42.9	<u>49.8</u>
	MLP	<b>35.4</b>	<b>43.0</b>	<b>50.0</b>
	NeuralODE	34.8	42.4	49.4
	NeuralSDE	34.9	42.6	49.3
SGA	IM	<b>28.2</b>	<b>36.5</b>	<b>45.5</b>
	MLP	<u>27.4</u>	<u>34.7</u>	<u>43.5</u>
	NeuralODE	16.5	25.1	36.8
	NeuralSDE	26.3	34.2	43.0
SGF	IM	<u>10.6</u>	<u>13.3</u>	<u>15.5</u>
	MLP	10.0	12.6	14.8
	NeuralODE	6.9	8.5	10.0
	NeuralSDE	<b>11.3</b>	<b>13.6</b>	<b>16.4</b>

**Realization of the LDM.** We evaluate different instantiations of the Location Dynamics Model (LDM) from Eq. (4)

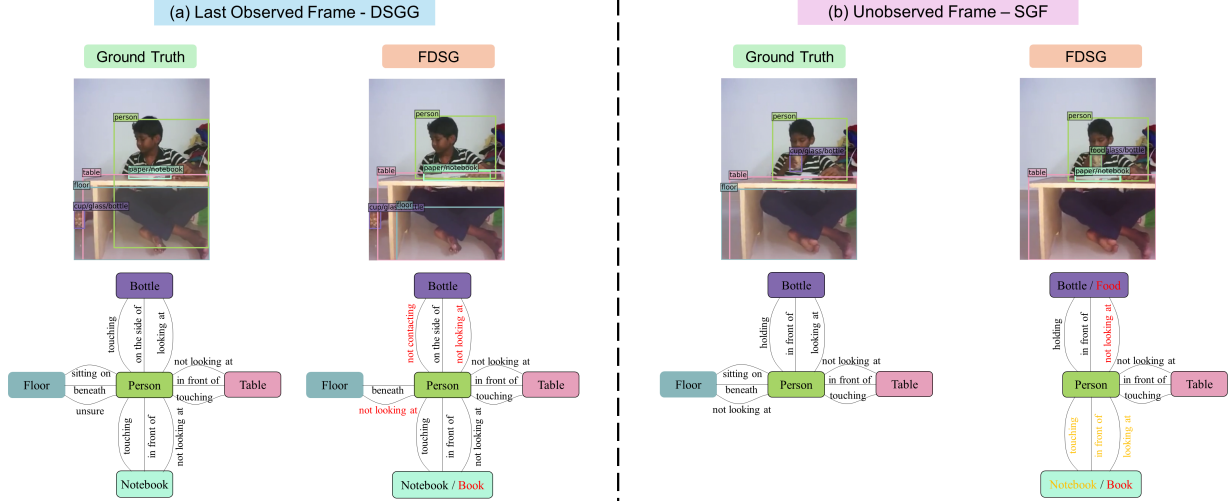


Figure 4. Visualization of Dynamic Scene Graph Generation (DSGG) and Scene Graph Forecasting (SGF) outputs of our proposed method. The first row shows frames and ground truth / predicted entity bounding boxes, while the second row shows corresponding scene graphs. In the scene graphs, incorrect predicates are highlighted with text in red, while entities / predicates with missing labels in the ground truth are highlighted in orange. For (a) observed frames, we provide our DSGG results and compare with the ground truth. For (b) unobserved frames, we contrast our SGF results to the ground truth.

with results summarized in Table 5. When using residual updates for entity location representations (Eq. (6)), the Triplet Dynamics Model (TDM) also predicts these residuals. We hypothesize that this coupling helps TDM better model predicate dynamics when they are linked to entity motion, which is supported by the observed performance trends. Among the variants, Identity Mapping offers the best overall performance: top in SGA, second-best in DSGG and SGF, with only marginal gaps from the top models in the latter two tasks. The 3-layer MLP achieves the best DSGG performance but underperforms in SGA. NeuralSDE excels in SGF, indicating stronger entity forecasting, but lags in DSGG and SGA, suggesting reduced effectiveness in predicate anticipation. Based on overall performance, simplicity, and compactness, Identity Mapping is adopted.

#### 4.4. Qualitative Results

We provide qualitative DSGG and SGF results of our proposed FDSG framework on a sample video from the Action Genome dataset in Fig. 4. For SGF, the observation fraction is  $\mathcal{F} = 0.7$ . The comparative evaluation demonstrates the superior performance of FDSG in both DSGG and SGF. Specifically, for DSGG, our model is able to detect all entities and infer most relationships correctly. For SGF, our model performs remarkably well in modeling both static (e.g. the table) and dynamic (e.g. the bottle) entities. The movement of the bottle from the left to the center is correctly captured and its bounding box precisely forecasted, while bounding boxes for the person, table, and notebook remain unchanged. This demonstrates the effectiveness of our proposed Location Dynamics Model using Identity Mapping for the query locations. It is also noteworthy that

FDSG is capable of forecasting new objects which can potentially and reasonably interact with the central person, e.g. *person-holding-food*. This shows that FDSG has developed a comprehensive understanding of the video which allows the model to foresee upcoming actions. On the other hand, however, these emerging entities might take up limited entity queries, leading the model to ignore background information such as the floor. We provide more qualitative results in Supplementary D, and visualization of attention maps for DSGG.

#### 5. Conclusion

In this work, we introduce Forecasting Dynamic Scene Graph (FDSG), a novel framework extending Dynamic Scene Graph Generation (DSGG) by incorporating extrapolation to predict future relationships, entity labels, and bounding boxes. In contrast to the existing DSGG methods relying solely on interpolation, FDSG employs a Forecast Module with query decomposition and NeuralSDE, alongside a Temporal Aggregation Module that integrates forecasted scene graphs with observed frames to enhance scene graph generation. To evaluate FDSG, we propose Scene Graph Forecasting (SGF), a new task assessing the prediction of complete future scene graphs. Experiments on the Action Genome dataset demonstrate FDSG’s superior performance across DSGG, SGA, and SGF tasks. Significant improvements over baselines validate the effectiveness of our method and the benefits of learning to extrapolate. Our findings suggest that extrapolation enhances both forecasting and overall scene understanding, paving the way for future research on e.g., long-term scene prediction in video understanding and action recognition.



## References

- [1] Jingwei Cao, Hongyu Zhang, Lisheng Jin, Jiawang Lv, Guoyang Hou, and Chengtao Zhang. A review of object tracking methods: From general field to autonomous vehicles. *Neurocomputing*, 2024. 3
- [2] Nicolas Carion, Francisco Massa, Gabriel Synnaeve, Nicolas Usunier, Alexander Kirillov, and Sergey Zagoruyko. End-to-end object detection with transformers. In *European conference on computer vision*, pages 213–229. Springer, 2020. 2, 5
- [3] Xiaojun Chang, Pengzhen Ren, Pengfei Xu, Zhihui Li, Xiaojiang Chen, and Alex Hauptmann. A comprehensive survey of scene graphs: Generation and application. *IEEE Transactions on Pattern Analysis and Machine Intelligence*, 45(1): 1–26, 2021. 5
- [4] Yupeng Chang, Xu Wang, Jindong Wang, Yuan Wu, Linyi Yang, Kaijie Zhu, Hao Chen, Xiaoyuan Yi, Cunxiang Wang, Yidong Wang, et al. A survey on evaluation of large language models. *ACM Transactions on Intelligent Systems and Technology*, 15(3):1–45, 2024. 2
- [5] Ricky TQ Chen, Yulia Rubanova, Jesse Bettencourt, and David K Duvenaud. Neural ordinary differential equations. *Advances in neural information processing systems*, 31, 2018. 3
- [6] Yuting Chen, Joseph Wang, Yannan Bai, Gregory Castañón, and Venkatesh Saligrama. Probabilistic semantic retrieval for surveillance videos with activity graphs. *IEEE Transactions on Multimedia*, 21(3):704–716, 2018. 1
- [7] Anoop Cherian, Chiori Hori, Tim K Marks, and Jonathan Le Roux. (2.5+ 1) d spatio-temporal scene graphs for video question answering. In *Proceedings of the AAAI Conference on Artificial Intelligence*, pages 444–453, 2022. 1
- [8] Hyung-gun Chi, Kwonjoon Lee, Nakul Agarwal, Yi Xu, Karthik Ramani, and Chihoh Choi. Adamsformer for spatial action localization in the future. In *Proceedings of the IEEE/CVF Conference on Computer Vision and Pattern Recognition*, pages 17885–17895, 2023. 3, 5
- [9] Yuren Cong, Wentong Liao, Hanno Ackermann, Bodo Rosenhahn, and Michael Ying Yang. Spatial-temporal transformer for dynamic scene graph generation. In *Proceedings of the IEEE/CVF international conference on computer vision*, pages 16372–16382, 2021. 1, 2, 4, 6, 13, 14, 15, 16
- [10] Yuren Cong, Michael Ying Yang, and Bodo Rosenhahn. Reltr: Relation transformer for scene graph generation. *IEEE Transactions on Pattern Analysis and Machine Intelligence*, 45(9):11169–11183, 2023. 2, 12
- [11] Shengyu Feng, Hesham Mostafa, Marcel Nassar, Somdeb Majumdar, and Subarna Tripathi. Exploiting long-term dependencies for generating dynamic scene graphs. In *Proceedings of the IEEE/CVF Winter Conference on Applications of Computer Vision*, pages 5130–5139, 2023. 2, 6, 13, 14, 15, 16
- [12] Harshala Gammulle, Simon Denman, Sridha Sridharan, and Clinton Fookes. Predicting the future: A jointly learnt model for action anticipation. In *Proceedings of the IEEE/CVF International Conference on Computer Vision*, pages 5562–5571, 2019. 3
- [13] Dayoung Gong, Joonseok Lee, Manjin Kim, Seong Jong Ha, and Minsu Cho. Future transformer for long-term action anticipation. In *Proceedings of the IEEE/CVF Conference on Computer Vision and Pattern Recognition*, pages 3052–3061, 2022. 3
- [14] Kaiming He, Xiangyu Zhang, Shaoqing Ren, and Jian Sun. Deep residual learning for image recognition. In *Proceedings of the IEEE conference on computer vision and pattern recognition*, pages 770–778, 2016. 6
- [15] Jinbae Im, JeongYeon Nam, Nokyoung Park, Hyungmin Lee, and Seunghyun Park. Egtr: Extracting graph from transformer for scene graph generation. In *Proceedings of the IEEE/CVF Conference on Computer Vision and Pattern Recognition*, pages 24229–24238, 2024. 2, 4, 12
- [16] Jingwei Ji, Ranjay Krishna, Li Fei-Fei, and Juan Carlos Niebles. Action genome: Actions as compositions of spatio-temporal scene graphs. In *Proceedings of the IEEE/CVF Conference on Computer Vision and Pattern Recognition*, pages 10236–10247, 2020. 2, 5
- [17] Jingwei Ji, Rishi Desai, and Juan Carlos Niebles. Detecting human-object relationships in videos. In *Proceedings of the IEEE/CVF international conference on computer vision*, pages 8106–8116, 2021. 1, 2
- [18] Justin Johnson, Ranjay Krishna, Michael Stark, Li-Jia Li, David Shamma, Michael Bernstein, and Li Fei-Fei. Image retrieval using scene graphs. In *Proceedings of the IEEE conference on computer vision and pattern recognition*, pages 3668–3678, 2015. 1
- [19] Oluwafunmilola Kesa, Olly Styles, and Victor Sanchez. Multiple object tracking and forecasting: Jointly predicting current and future object locations. In *Proceedings of the IEEE/CVF Winter Conference on Applications of Computer Vision*, pages 560–569, 2022. 3
- [20] Patrick Kidger, James Foster, Xuechen Chen Li, and Terry Lyons. Efficient and accurate gradients for neural sdes. *Advances in Neural Information Processing Systems*, 34: 18747–18761, 2021. 2, 11
- [21] Yu Kong and Yun Fu. Human action recognition and prediction: A survey. *International Journal of Computer Vision*, 130(5):1366–1401, 2022. 1
- [22] Hongsheng Li, Guangming Zhu, Liang Zhang, Youliang Jiang, Yixuan Dang, Haoran Hou, Peiyi Shen, Xia Zhao, Syed Afaq Ali Shah, and Mohammed Bennamoun. Scene graph generation: A comprehensive survey. *Neurocomputing*, 566:127052, 2024. 5
- [23] Rongjie Li, Songyang Zhang, and Xuming He. Sgtr: End-to-end scene graph generation with transformer. In *proceedings of the IEEE/CVF conference on computer vision and pattern recognition*, pages 19486–19496, 2022. 2
- [24] Yiming Li, Xiaoshan Yang, and Changsheng Xu. Dynamic scene graph generation via anticipatory pre-training. In *Proceedings of the IEEE/CVF conference on computer vision and pattern recognition*, pages 13874–13883, 2022. 2, 6, 13
- [25] Tsung-Yi Lin, Michael Maire, Serge Belongie, James Hays, Pietro Perona, Deva Ramanan, Piotr Dollár, and C Lawrence Zitnick. Microsoft coco: Common objects in context. In *European Conference on Computer Vision*, pages 740–755, 2014. 6

- [26] Xin Lin, Changxing Ding, Jinquan Zeng, and Dacheng Tao. Gps-net: Graph property sensing network for scene graph generation. In *Proceedings of the IEEE/CVF Conference on Computer Vision and Pattern Recognition*, pages 3746–3753, 2020. [2](#), [6](#), [13](#)
- [27] Xin Lin, Changxing Ding, Jing Zhang, Yibing Zhan, and Dacheng Tao. Ru-net: Regularized unrolling network for scene graph generation. In *Proceedings of the IEEE/CVF Conference on Computer Vision and Pattern Recognition*, pages 19457–19466, 2022. [2](#)
- [28] Yixin Liu, Kai Zhang, Yuan Li, Zhiling Yan, Chujie Gao, Ruoxi Chen, Zhengqing Yuan, Yue Huang, Hanchi Sun, Jianfeng Gao, et al. Sora: A review on background, technology, limitations, and opportunities of large vision models. *arXiv preprint arXiv:2402.17177*, 2024. [2](#)
- [29] Ilya Loshchilov and Frank Hutter. Decoupled weight decay regularization. *arXiv preprint arXiv:1711.05101*, 2017. [12](#)
- [30] Sayak Nag, Kyle Min, Subarna Tripathi, and Amit K Roy-Chowdhury. Unbiased scene graph generation in videos. In *Proceedings of the IEEE/CVF Conference on Computer Vision and Pattern Recognition*, pages 22803–22813, 2023. [6](#), [12](#), [13](#)
- [31] Megha Nawhal, Akash Abdu Jyothi, and Greg Mori. Rethinking learning approaches for long-term action anticipation. In *European Conference on Computer Vision*, pages 558–576. Springer, 2022. [3](#)
- [32] Trong-Thuan Nguyen, Pha Nguyen, and Khoa Luu. Hig: Hierarchical interlacement graph approach to scene graph generation in video understanding. In *Proceedings of the IEEE/CVF Conference on Computer Vision and Pattern Recognition*, pages 18384–18394, 2024. [1](#)
- [33] Rohith Peddi, Saksham Singh, Parag Singla, Vibhav Gogate, et al. Towards scene graph anticipation. In *European Conference on Computer Vision*, pages 159–175. Springer, 2024. [2](#), [4](#), [5](#), [6](#), [7](#), [12](#), [13](#), [14](#), [15](#), [16](#)
- [34] Shaoqing Ren, Kaiming He, Ross Girshick, and Jian Sun. Faster r-cnn: Towards real-time object detection with region proposal networks. *IEEE transactions on pattern analysis and machine intelligence*, 39(6):1137–1149, 2016. [2](#)
- [35] Cristian Rodriguez, Basura Fernando, and Hongdong Li. Action anticipation by predicting future dynamic images. In *Proceedings of the European Conference on Computer Vision (ECCV) Workshops*, 2018. [3](#)
- [36] T-YLPG Ross and GKHP Dollár. Focal loss for dense object detection. In *proceedings of the IEEE conference on computer vision and pattern recognition*, pages 2980–2988, 2017. [5](#)
- [37] Oliver Styles, Victor Sanchez, and Tanaya Guha. Multiple object forecasting: Predicting future object locations in diverse environments. In *Proceedings of the IEEE/CVF Winter Conference on Applications of Computer Vision*, pages 690–699, 2020. [3](#)
- [38] Kaihua Tang, Hanwang Zhang, Baoyuan Wu, Wenhan Luo, and Wei Liu. Learning to compose dynamic tree structures for visual contexts. In *Proceedings of the IEEE/CVF conference on computer vision and pattern recognition*, pages 6619–6628, 2019. [6](#), [13](#)
- [39] Kaihua Tang, Yulei Niu, Jianqiang Huang, Jiaxin Shi, and Hanwang Zhang. Unbiased scene graph generation from biased training. In *Proceedings of the IEEE/CVF conference on computer vision and pattern recognition*, pages 3716–3725, 2020. [2](#)
- [40] Yao Teng, Limin Wang, Zhifeng Li, and Gangshan Wu. Target adaptive context aggregation for video scene graph generation. In *Proceedings of the IEEE/CVF International Conference on Computer Vision*, pages 13688–13697, 2021. [1](#), [2](#), [6](#), [13](#)
- [41] Guan Wang, Zhimin Li, Qingchao Chen, and Yang Liu. Oed: Towards one-stage end-to-end dynamic scene graph generation. In *Proceedings of the IEEE/CVF Conference on Computer Vision and Pattern Recognition*, pages 27938–27947, 2024. [2](#), [4](#), [5](#), [6](#), [11](#), [12](#), [13](#)
- [42] Jingyi Wang, Jinfa Huang, Can Zhang, and Zhidong Deng. Cross-modality time-variant relation learning for generating dynamic scene graphs. In *2023 IEEE International Conference on Robotics and Automation (ICRA)*, pages 8231–8238. IEEE, 2023. [1](#), [2](#)
- [43] Danfei Xu, Yuke Zhu, Christopher B Choy, and Li Fei-Fei. Scene graph generation by iterative message passing. In *Proceedings of the IEEE conference on computer vision and pattern recognition*, pages 5410–5419, 2017. [2](#)
- [44] Jia Xu, René Ranftl, and Vladlen Koltun. Accurate optical flow via direct cost volume processing. In *Proceedings of the IEEE Conference on Computer Vision and Pattern Recognition*, pages 1289–1297, 2017. [3](#)
- [45] Rowan Zellers, Mark Yatskar, Sam Thomson, and Yejin Choi. Neural motifs: Scene graph parsing with global context. In *Proceedings of the IEEE conference on computer vision and pattern recognition*, pages 5831–5840, 2018. [2](#)
- [46] Hao Zhang, Feng Li, Shilong Liu, Lei Zhang, Hang Su, Jun Zhu, Lionel M Ni, and Heung-Yeung Shum. Dino: Detr with improved denoising anchor boxes for end-to-end object detection. *arXiv preprint arXiv:2203.03605*, 2022. [2](#), [4](#)
- [47] Ji Zhang, Kevin J Shih, Ahmed Elgammal, Andrew Tao, and Bryan Catanzaro. Graphical contrastive losses for scene graph parsing. In *Proceedings of the IEEE/CVF Conference on Computer Vision and Pattern Recognition*, pages 11535–11543, 2019. [6](#), [13](#)
- [48] Yong Zhang, Yingwei Pan, Ting Yao, Rui Huang, Tao Mei, and Chang-Wen Chen. End-to-end video scene graph generation with temporal propagation transformer. *IEEE Transactions on Multimedia*, 26:1613–1625, 2023. [1](#), [2](#)
- [49] Qianyu Zhou, Xiangtai Li, Lu He, Yibo Yang, Guangliang Cheng, Yunhai Tong, Lizhuang Ma, and Dacheng Tao. Transvot: End-to-end video object detection with spatial-temporal transformers. *IEEE Transactions on Pattern Analysis and Machine Intelligence*, 45(6):7853–7869, 2022. [4](#)
- [50] Xizhou Zhu, Weijie Su, Lewei Lu, Bin Li, Xiaogang Wang, and Jifeng Dai. Deformable detr: Deformable transformers for end-to-end object detection. In *International Conference on Learning Representations*, 2021. [14](#)

## Supplementary Materials

### A. Overview

As presented in the main paper, we propose Forecasting Dynamic Scene Graphs (FDSG), a novel framework that extends Dynamic Scene Graph Generation (DSGG) by incorporating extrapolation to predict future scene graphs. We also propose a novel task called Scene Graph Forecasting (SGF) to evaluate FDSG’s capability to anticipate scene graphs. In these supplementary materials, we present more details of the proposed model and further evaluation results. Section B provides details of FDSG, including precise operations in the Transformer layers, the progressive temporal aggregation technique in our Temporal Aggregation Module, more details of NeuralSDE utilized in the Triplet Dynamics Model, the configurations of model training, and the implementation of SceneSayer+ as a baseline for the SGF task.

Section C presents more evaluation results, including Predicate Classification (PredCLS) and Scene Graph Classification (SGCLS) results on the DSGG task; and Action Genome Scenes (AGS), Partially Grounded Action Genome Scenes (PGAGS), and Grounded Action Genome Scenes (GAGS) results on the SGA task. Evaluation results for SGA and SGF tasks with different anticipatory horizons  $\mathcal{F}$  are presented. Our ablation study is supplemented with the results under more evaluation metrics. We also provide an ablation study on alternative strategies for temporal aggregation. In addition, we evaluate entity forecasting and present detailed results.

### B. Implementation Details

#### B.1. Transformer Layers

Transformers use attention mechanisms to compute contextual representations of input tokens. The two main types are self-attention (SelfAttn) and cross-attention (CrossAttn).

In self-attention, each token in the input attends to all other tokens in the same sequence. Given an input sequence  $X \in \mathbb{R}^{n \times d}$ , where  $n$  is the sequence length and  $d$  is the hidden size, we compute:

$$Q = XW^Q, \quad K = XW^K, \quad V = XW^V \quad (14)$$

$$\text{SelfAttn}(Q, K, V) = \text{softmax}\left(\frac{QK^\top}{\sqrt{d_k}}\right)V \quad (15)$$

where  $W^Q, W^K, W^V \in \mathbb{R}^{d \times d_k}$  are learned projection matrices, and  $d_k$  is the dimensionality of the keys and queries. The scaled dot-product attention computes a weighted sum of the values  $V$ .

In cross-attention (used in encoder-decoder architectures), the query comes from one sequence (e.g., the decoder input), while keys and values come from another

(e.g., the encoder output). Let  $X_{\text{query}} \in \mathbb{R}^{m \times d}$  and  $X_{\text{context}} \in \mathbb{R}^{n \times d}$ :

$$Q = X_{\text{query}}W^Q, \quad K = X_{\text{context}}W^K, \quad V = X_{\text{context}}W^V \quad (16)$$

$$\text{CrossAttn}(Q, K, V) = \text{softmax}\left(\frac{QK^\top}{\sqrt{d_k}}\right)V \quad (17)$$

In Eqs. (9) and (10),  $\text{SelfAttn}(Z_{T_g})$  means the input sequence  $X = Z_{T_g}$ , where  $Z_{T_g} \in \mathbb{R}^{100 \times 512}$ , i.e., each triplet representation  $Z$  has 512d, with 100 triplets in total.  $\text{CrossAttn}(\text{SelfAttn}(Z_{T_g}), \text{TopK}(Z_{\text{ref}}, k))$  means  $X_{\text{query}} = \text{SelfAttn}(Z_{T_g})$  and  $X_{\text{context}} = \text{TopK}(Z_{\text{ref}}, k)$ . Similarly,  $\text{CrossAttn}(\text{SelfAttn}(Z_{T_g}), Z_{T_0+\Delta T})$  means  $X_{\text{query}} = \text{SelfAttn}(Z_{T_g})$  and  $X_{\text{context}} = Z_{T_0+\Delta T}$ .

#### B.2. Progressive Refinement in Temporal Aggregation Module

In our Temporal Aggregation Module, to integrate information from reference frames with the target frame, we follow OED [41] and use cascaded Cross-attention layers for progressive refinement. Specifically, with multiple layers and gradually decreasing  $k$ , the process described in Eq. (9) in the main paper can be more rigorously formulated as:

$$Z_{T_0}^{(i)} = \text{CrossAttn}(\text{SelfAttn}(Z_{T_0}^{(i-1)}), Z_{\text{ref}}^{(i)}), \quad (18)$$

$$Z_{\text{ref}}^{(i)} = \text{TopK}(Z_{\text{ref}}^{(i-1)}, k_i), \quad (19)$$

where  $i$  denotes the  $i$ -th Cross-attention layer. In our implementation, we set the total number of layers to 3.

#### B.3. NeuralSDE

A NeuralSDE models an initial value problem with drift and diffusion terms, with each term being parameterized by a neural network [20]. In our FDSG, the Triplet Dynamics Model uses a NeuralSDE to predict the evolution of triplets, from the initial state  $z_{T_0}$  at time  $T_0$  to the target state  $z_{T_0+\Delta T}$  over the prediction time horizon  $\Delta T$ :

$$\begin{aligned} z_{T_0+\Delta T} &= \text{NeuralSDE}(z_{T_0}, \Delta T; \theta_c, \phi_c, W_c) \\ &= z_{T_0} + \int_{T_0}^{T_0+\Delta T} \mu_{\theta_c}(z_{T_0}) dt \\ &\quad + \int_{T_0}^{T_0+\Delta T} \nu_{\phi_c}(z_{T_0}) dW_c(t). \end{aligned} \quad (20)$$

where  $\mu_{\theta_c}(\cdot)$ ,  $\nu_{\phi_c}(\cdot)$ , and  $W_c(\cdot)$  denote drift terms parameterized by  $\theta_c$ , diffusion terms parameterized by  $\phi_c$ , and a Wiener process, respectively. Both  $\mu_{\theta_c}(\cdot)$  and  $\nu_{\phi_c}(\cdot)$  are three-layer MLPs, with the hidden layer dimension being 2,048 and Tanh as the activation function.

## B.4. Model Training

Following OED [41], we first pre-trained the Scene Graph Generation baseline and then fine-tuned the Temporal Aggregation Module together with the Forecast Module. The Scene Graph Generation baseline was trained for 5 epochs with a starting learning rate of 0.0001 and being reduced by a factor of 0.1 at the 4th epoch. We used AdamW [29] as optimizer with a batch size of 2. The temporal and forecast modules were fine-tuned for 3 epochs, with a starting learning rate of 0.0001, batch size of 1, and reduced learning rate by a factor of 0.1 at the 3rd epoch. The weighting factors  $\alpha_l$  and  $\beta_l$  in the matching loss (Eq. (13) in the main text) are 1.0 and 5.0, respectively. We used 8 NVIDIA GeForce RTX-2080Ti GPUs for training and evaluation.

## B.5. Implementation of SceneSayer+

We use the anticipated relationship representations of SceneSayer LDPU [33] to regress bounding boxes for the corresponding entities. Specifically, we feed the anticipated relationship representations  $z_{T_0+\Delta T}(i, j)$  to two 3-layer MLPs, one for subject bounding box regression and one for object:

$$\hat{b}_{T_0+\Delta T}(i) = \text{MLP}_{\text{sub}}(z_{T_0+\Delta T}(i, j)), \quad (21)$$

$$\hat{b}_{T_0+\Delta T}(j) = \text{MLP}_{\text{obj}}(z_{T_0+\Delta T}(i, j)), \quad (22)$$

where both MLPs have a hidden layer dimension of 1,024, with ReLU as the intermediate activation function and Soft-Plus as the last activation function.

We use the smoothed  $L_1$  loss for the bounding box anticipation error:

$$\mathcal{L}_{\text{box}}^T = \sum_{t=T+1}^H \sum_{k \in \text{entities}} \mathcal{L}_{l_1 \text{smooth}}(\hat{b}_t(k), b_t(k)) \quad (23)$$

while other loss terms remain the same as in SceneSayer.  $T$  denotes the last observed time step and  $H$  denotes the last frame in the given video. It should be noted that this bounding box loss is mentioned in the paper of SceneSayer [33]). However, we did not find the implementation of this bounding box loss in their open-source code. Hence, we followed the ideas described in the paper and implemented our baseline SceneSayer+ for the SGF task.

## C. Detailed Evaluation Results

### C.1. PredCLS and SGCLS

We provide evaluation results for Predicate Classification (PredCLS) and Scene Graph Classification (SGCLS) for the DSGG task in Table 6 and Table 7, respectively. PredCLS aims to classify the predicate labels with ground-truth bounding boxes and labels of the entities being given, while SGCLS aims to classify entity and predicate labels with

only ground-truth bounding boxes being given. Both PredCLS and SGCLS are less challenging than Scene Graph Detection (SGDET) (reported in the main paper), which requires predicting entity labels, bounding boxes, and predicates.

It is worth mentioning that unlike OED [41], we do not train separate models for the PredCLS and SGCLS tasks. We follow the recently verified match-and-assign strategy in one-stage scene graph generation methods [10, 15], the ground-truth labels can be easily assigned to the queries with matched triplet proposals for the evaluation of PredCLS and SGCLS. In contrast, OED follows the two-stage model strategy that the model is modified to incorporate additional input information (ground truth bounding boxes in SGCLS and additionally ground truth bounding box and entity labels in PredCLS) and then re-trained.

For PredCLS, our model achieves comparable performance to the state-of-the-art model OED, even without training a separate model for PredCLS. For SGCLS, in general, our model outperforms other baselines, especially TEMPURA [30], which is specifically designed for unbiased scene graph generation on the Mean Recall metrics. Since the SGCLS results of OED are not reported in the paper [41] and the model checkpoint is unavailable, we have to exclude OED in Table 7. The strong performance of our FDSG method on PredCLS and SGCLS is consistent with SGDET results reported in the main paper, demonstrating the overall superiority of FDSG on the DSGG task.

### C.2. Different Observation Fractions

Following [33], we provided further results for Scene Graph Anticipation (SGA) on the Action Genome Scenes (AGS) (Table 8), Partially Grounded Action Genome Scenes (PGAGS) (Table 9), and Grounded Action Genome Scenes (GAGS) (Table 10). AGS resembles SGDET, where the model only sees video frames and predicts future scene graphs without bounding boxes. Similarly, GAGS aims to anticipate predicate labels, given ground-truth bounding boxes and labels of the entities. PGAGS aims to classify entity and predicate labels with ground-truth bounding boxes given. To provide a more detailed analysis about the anticipation capacity, we evaluate our model under different observation fractions of the video, *i.e.*,  $\mathcal{F} = 0.3, 0.5, 0.7, 0.9$ .

In all three tasks, our model consistently outperforms existing methods in different observation fractions. In AGS and GAGS, our model significantly outperforms the baselines. In PGAGS, while SceneSayer [33] marginally outperforms our model on the Recall metrics under the No Constraint setting, FDSG performs notably better than SceneSayer on the Mean Recall metrics, which gives the same indication as the SGA results presented in the main paper that our model has excellent capability of unbiased scene graph generation. These results demonstrate the superiority



Table 6. Comparison with state-of-the-art Dynamic Scene Graph Generation methods on Action Genome for **Predicate Classification (PredCLS)**. Best and second best values are highlighted in **boldface** and underlined, respectively.

PredCLS	Recall@K (R@K) $\uparrow$						Mean Recall@K (mR@K) $\uparrow$					
	With Constraint			No Constraint			With Constraint			No Constraint		
Method	10	20	50	10	20	50	10	20	50	10	20	50
RelDN [47]	66.3	69.5	69.5	75.7	93.0	99.0	6.2	6.2	6.2	31.2	63.1	75.5
VCTree [38]	66.0	69.3	69.3	75.5	92.9	99.3	-	-	-	-	-	-
TRACE [40]	27.5	27.5	27.5	72.6	91.6	96.4	15.2	15.2	15.2	50.9	73.6	82.7
GPS-Net [26]	66.8	69.9	69.9	76.0	93.6	<b>99.5</b>	-	-	-	-	-	-
STTran [9]	68.6	71.8	71.8	77.9	94.2	99.1	37.8	40.1	40.2	51.4	67.7	82.7
APT [24]	69.4	73.8	73.8	78.5	95.1	99.2	-	-	-	-	-	-
TEMPURA [30]	68.8	71.5	71.5	80.4	94.2	99.4	<b>42.9</b>	<b>46.3</b>	<b>46.3</b>	<b>61.5</b>	<b>85.1</b>	<b>98.0</b>
OED [41]	<b>73.0</b>	<b>76.1</b>	<b>76.1</b>	<b>83.3</b>	<u>95.3</u>	99.2	-	-	-	-	-	-
Ours	<u>72.9</u>	<u>75.9</u>	<u>75.9</u>	<u>83.2</u>	<b>95.4</b>	99.4	<u>41.0</u>	<u>44.7</u>	<u>44.8</u>	<u>56.7</u>	<u>83.3</u>	<u>97.7</u>

Table 7. Comparison with state-of-the-art Dynamic Scene Graph Generation methods on Action Genome for **Scene Graph Classification (SGCLS)**. Best and second best values are highlighted in **boldface** and underlined, respectively.

SGCLS	Recall@K (R@K) $\uparrow$						Mean Recall@K (mR@K) $\uparrow$					
	With Constraint			No Constraint			With Constraint			No Constraint		
Method	10	20	50	10	20	50	10	20	50	10	20	50
RelDN [47]	44.3	45.4	45.4	52.9	62.4	65.1	3.3	3.3	3.3	7.5	18.8	33.7
VCTree [38]	44.1	45.3	45.3	52.4	62.0	65.1	-	-	-	-	-	-
TRACE [40]	-	45.7	46.8	-	-	-	8.9	8.9	8.9	31.9	42.7	46.3
GPS-Net [26]	45.3	46.5	46.5	53.6	63.3	66.0	-	-	-	-	-	-
STTran [9]	46.4	47.5	47.5	54.0	63.7	66.4	16.6	20.8	22.2	20.9	29.7	39.2
APT [24]	47.2	48.9	48.9	55.1	65.1	68.7	-	-	-	-	-	-
DSG-DETR [11]	<u>50.8</u>	<u>52.0</u>	<u>52.0</u>	<b>59.2</b>	<b>69.1</b>	<b>72.4</b>	-	-	-	-	-	-
TEMPURA [30]	47.2	48.3	48.3	56.3	64.7	67.9	<u>30.4</u>	<u>35.2</u>	<u>35.2</u>	<u>48.3</u>	<u>61.1</u>	<u>66.4</u>
Ours	<b>54.8</b>	<b>56.5</b>	<b>56.5</b>	<u>59.0</u>	<u>67.2</u>	<b>72.4</b>	<b>34.9</b>	<b>36.8</b>	<b>36.8</b>	<b>48.9</b>	<b>63.8</b>	<b>74.0</b>

of FDSG in both short-term SGA ( $\mathcal{F} = 0.9$ ) and long-term SGA ( $\mathcal{F} = 0.3$ ).

Moreover, in AGS, it is evident that the performance gain of our FDSG (e.g., mR@10 No Constraint increases from 41.7 to 59.5) is more profound than that of the runner-up model SceneSayerSDE [33] (e.g., mR@10 No Constraint increases from 37.1 to 46.8) with the observation fraction increasing from 0.3 to 0.9. A similar increasing trend can be observed in PGAGS and GAGS. This clearly demonstrates that our model is more capable of learning to extrapolate, which in turn largely benefits the performance of scene understanding in videos.

In addition, in AGS, the performance gap between SceneSayerSDE and FDSG (e.g., 10.9 in R@20 With Constraint with  $\mathcal{F} = 0.9$ ) is clearly greater than that in PGAGS (3.5) and GAGS (3.1). Since in PGAGS and GAGS ground truth bounding boxes are given, this finding provides further support that learning to forecast entity bounding boxes

benefits the performance of FDSG.

We also evaluate our model’s performance on SGF with different observed fractions of the video  $\mathcal{F} = 0.3, 0.5, 0.7, 0.9$ , which is presented in Table 11. FDSG consistently outperforms baseline models under all settings, demonstrating the superiority and robustness of our model’s capability to forecast scene graphs.

### C.3. More Ablation Study

In Tables 12 and 13, we provide details of the ablation study on the effectiveness of different model components. Results obtained under the additional evaluation metrics are consistent with what we have observed with R@20. Either the Temporal Aggregation Module or the Scene Graph Forecast module can benefit all the DSGG, SGA and SGF tasks, indicating that by combining these modules together our model learns a more comprehensive understanding of the scene and video.

Table 8. Comparison with state-of-the-art Scene Graph Anticipation methods on **Action Genome Scenes (AGS)**. Best and second best values are highlighted in **boldface** and underlined, respectively.

$\mathcal{F}$	Method	Recall@K (R@K) $\uparrow$						Mean Recall@K (mR@K) $\uparrow$					
		With Constraint			No Constraint			With Constraint			No Constraint		
		10	20	50	10	20	50	10	20	50	10	20	50
0.3	STTran++ [9, 33]	18.5	27.9	29.5	15.4	27.2	48.6	5.9	10.4	11.3	6.2	14.1	31.2
	DSG-DETR++ [11, 33]	19.5	28.3	29.4	16.8	29.0	<b>48.9</b>	6.0	10.3	11.0	8.4	16.7	32.3
	SceneSayerODE [33]	23.1	29.2	31.4	23.3	32.5	45.1	10.6	13.8	15.0	13.3	20.1	33.0
	SceneSayerSDE [33]	<u>25.0</u>	<u>31.7</u>	<u>34.3</u>	<u>25.9</u>	<u>35.0</u>	47.4	<u>11.4</u>	<u>15.3</u>	<u>16.9</u>	<u>15.6</u>	<u>23.1</u>	<u>37.1</u>
	Ours	<b>26.8</b>	<b>34.2</b>	<b>43.0</b>	<b>27.8</b>	<b>37.6</b>	<u>48.7</u>	<b>15.4</b>	<b>20.2</b>	<b>24.7</b>	<b>18.3</b>	<b>29.8</b>	<b>41.7</b>
0.5	STTran++ [9, 33]	19.7	30.2	31.8	16.6	29.1	51.5	6.3	11.3	12.3	6.6	14.7	33.4
	DSG-DETR++ [11, 33]	20.7	30.3	31.6	17.4	30.5	<u>51.9</u>	6.4	11.0	11.7	8.4	17.0	33.9
	SceneSayerODE [33]	25.9	32.6	34.8	26.4	36.6	49.8	11.6	15.2	16.4	14.3	21.4	36.0
	SceneSayerSDE [33]	<u>27.3</u>	<u>34.8</u>	<u>37.0</u>	<u>28.4</u>	<u>38.6</u>	51.4	<u>12.4</u>	<u>16.6</u>	<u>18.0</u>	<u>16.3</u>	<u>25.1</u>	<u>39.9</u>
	Ours	<b>28.3</b>	<b>36.5</b>	<b>45.3</b>	<b>30.1</b>	<b>40.4</b>	<b>52.2</b>	<b>18.1</b>	<b>23.5</b>	<b>27.5</b>	<b>23.2</b>	<b>34.3</b>	<b>45.8</b>
0.7	STTran++ [9, 33]	22.1	33.6	35.2	19.0	32.8	<u>56.8</u>	7.0	12.6	13.6	7.7	17.1	36.8
	DSG-DETR++ [11, 33]	22.9	33.6	34.9	19.8	34.1	56.7	7.1	12.6	13.3	9.5	19.2	37.2
	SceneSayerODE [33]	30.3	36.6	38.9	32.1	42.8	55.6	12.8	16.4	17.8	16.5	24.4	39.6
	SceneSayerSDE [33]	<u>31.4</u>	<u>38.0</u>	<u>40.5</u>	<u>33.3</u>	<u>44.0</u>	56.4	<u>13.8</u>	<u>17.7</u>	<u>19.3</u>	<u>18.1</u>	<u>27.3</u>	<u>44.4</u>
	Ours	<b>35.5</b>	<b>43.9</b>	<b>50.6</b>	<b>37.1</b>	<b>49.2</b>	<b>60.2</b>	<b>21.6</b>	<b>27.9</b>	<b>31.2</b>	<b>25.0</b>	<b>41.9</b>	<b>54.7</b>
0.9	STTran++ [9, 33]	23.6	35.5	37.4	20.2	35.0	60.2	7.4	13.4	14.6	8.9	18.4	38.8
	DSG-DETR++ [11, 33]	24.4	36.1	37.6	22.2	37.1	61.0	7.4	13.8	14.8	11.4	21.0	39.5
	SceneSayerODE [33]	33.9	40.4	42.6	36.6	48.3	61.3	14.0	18.1	19.3	17.8	27.4	43.4
	SceneSayerSDE [33]	<u>34.8</u>	<u>41.9</u>	<u>44.1</u>	<u>37.3</u>	<u>48.6</u>	<u>61.6</u>	<u>15.1</u>	<u>19.4</u>	<u>21.0</u>	<u>20.8</u>	<u>30.9</u>	<u>46.8</u>
	Ours	<b>43.8</b>	<b>52.8</b>	<b>61.1</b>	<b>47.5</b>	<b>59.2</b>	<b>70.9</b>	<b>24.1</b>	<b>30.1</b>	<b>34.9</b>	<b>30.9</b>	<b>44.6</b>	<b>59.5</b>

In FDSG’s Temporal Aggregation Module, we first aggregate information from reference frames with lower uncertainty, followed by forecasts with higher uncertainty. In Table 14, we test two variants: (a) aggregating forecasts before observations, and (b) aggregating both information in a single cross-attention layer. Neither outperform our current design in FDSG.

#### C.4. Entity Detection

We use Object Detection Recall to assess how well predicted entities match the ground truth. We evaluate under two settings: (1) *SGA* where  $\text{IoU} \geq 0$ , *i.e.* only evaluates label accuracy; and (2) *SGF* where  $\text{IoU} \geq 0.5$ , *i.e.* includes bounding box quality. We compare against a *Baseline* using the predicted scene graph from the last observation and an *Oracle* using the last ground truth. We also report Average Precision (AP) with  $\text{IoU} \geq 0.5$  in Table 15. Our model clearly outperforms the *Baseline*, in particular in the *SGA* setting, showing promising capability to discover novel nodes. Our model sometimes closely trails the *Oracle* due to minor prediction errors for the last observation, and in the *SGF* setting due to accumulated error in label and bounding box prediction.

### D. Qualitative Results

#### D.1. Attention Maps

In Fig. 5, we visualize the sampling points of the Deformable Attention [50] in our FDSG’s entity decoder. The visualized sampling points are from the last Cross-Attention layer of the entity decoder. We show the top-5 most confident queries in terms of the overall classification score of entities and predicate. There are 128 sampling points associated with each query, and one attention weight associated with each sampling point. The larger attention weights are visualized in brighter color (*e.g.* yellow) while the smaller weights are shown in darker color (*e.g.* dark blue). Interestingly, the deformable attention not only attends to the entities, but also attempts to locate the interaction between the subject and the object. This is especially obvious in the first two columns, where the corresponding predicate is looking / not looking at, where the Attention mechanism concentrates around the direction where the central person is looking. We can also see that this direction is actually blocked by the table, which is possibly the reason that the model mistakenly predicts person – not looking at – bottle.

Table 9. Comparison with state-of-the-art Scene Graph Anticipation methods on Partially Grounded Action Genome Scenes (PGAGS). Best and second best values are highlighted in **boldface** and underlined, respectively.

$\mathcal{F}$	Method	Recall@K (R@K) $\uparrow$						Mean Recall@K (mR@K) $\uparrow$					
		With Constraint			No Constraint			With Constraint			No Constraint		
		10	20	50	10	20	50	10	20	50	10	20	50
0.3	STTran++ [9, 33]	22.1	22.8	22.8	28.1	39.0	45.2	9.2	9.8	9.8	17.7	30.6	42.0
	DSG-DETR++ [11, 33]	18.2	18.8	18.8	27.7	39.2	<b>47.3</b>	8.9	9.4	9.4	15.3	26.6	44.0
	SceneSayerODE [33]	27.0	27.9	27.9	33.0	40.9	46.5	12.9	13.4	13.4	19.4	27.9	46.9
	SceneSayerSDE [33]	28.8	29.9	29.9	34.6	<b>42.0</b>	46.2	<u>14.2</u>	<u>14.7</u>	<u>14.7</u>	<u>21.5</u>	<u>31.7</u>	48.2
	Ours	<b>31.3</b>	<b>32.4</b>	<b>32.4</b>	<b>35.2</b>	<u>41.8</u>	<u>47.1</u>	<b>20.6</b>	<b>21.8</b>	<b>21.8</b>	<b>28.9</b>	<b>40.8</b>	<b>51.4</b>
0.5	STTran++ [9, 33]	24.5	25.2	25.2	30.6	43.2	50.2	10.1	10.7	10.7	18.4	29.5	43.1
	DSG-DETR++ [11, 33]	20.7	21.4	21.4	30.4	44.0	<b>52.7</b>	10.2	10.8	10.8	16.5	30.8	45.1
	SceneSayerODE [33]	30.5	31.5	31.5	36.8	<u>45.9</u>	<u>51.8</u>	14.9	15.4	15.5	21.6	30.8	48.0
	SceneSayerSDE [33]	<u>32.2</u>	<u>33.3</u>	<u>33.3</u>	<b>38.4</b>	<b>46.9</b>	<u>51.8</u>	<u>15.8</u>	<u>16.6</u>	<u>16.6</u>	<u>23.5</u>	<u>35.0</u>	49.6
	Ours	<b>34.3</b>	<b>35.2</b>	<b>35.2</b>	<u>38.1</u>	45.0	50.5	<b>22.0</b>	<b>23.4</b>	<b>23.4</b>	<b>31.0</b>	<b>43.0</b>	<b>53.7</b>
0.7	STTran++ [9, 33]	29.1	29.7	29.7	36.8	51.6	58.7	11.5	12.1	12.1	21.2	34.6	49.0
	DSG-DETR++ [11, 33]	24.6	25.2	25.2	36.7	51.8	<b>60.6</b>	12.0	12.6	12.6	19.7	36.4	50.6
	SceneSayerODE [33]	36.5	37.3	37.3	<u>44.6</u>	<u>54.4</u>	<u>60.3</u>	16.9	17.3	17.3	25.2	36.2	53.1
	SceneSayerSDE [33]	<u>37.6</u>	<u>38.5</u>	<u>38.5</u>	<b>45.6</b>	<b>54.6</b>	59.3	<u>18.4</u>	<u>19.1</u>	<u>19.1</u>	<u>28.3</u>	<u>40.9</u>	<u>54.9</u>
	Ours	<b>39.9</b>	<b>40.7</b>	<b>40.7</b>	44.3	51.5	57.3	<b>24.7</b>	<b>25.9</b>	<b>25.9</b>	<b>33.8</b>	<b>47.7</b>	<b>58.1</b>
0.9	STTran++ [9, 33]	31.1	31.6	31.6	43.5	57.6	63.9	12.4	12.8	12.8	25.3	39.6	54.0
	DSG-DETR++ [11, 33]	27.6	28.1	28.1	45.8	61.5	<b>68.5</b>	13.2	13.7	13.7	25.8	42.9	58.3
	SceneSayerODE [33]	41.6	42.2	42.2	52.7	<u>61.8</u>	<u>66.5</u>	19.0	19.4	19.4	29.4	42.2	59.2
	SceneSayerSDE [33]	<u>42.5</u>	<u>43.1</u>	<u>43.1</u>	<b>53.8</b>	<b>62.4</b>	66.2	<u>20.6</u>	<u>21.1</u>	<u>21.1</u>	<u>32.9</u>	<u>46.0</u>	<u>59.8</u>
	Ours	<b>45.9</b>	<b>46.6</b>	<b>46.6</b>	<u>53.0</u>	60.0	64.7	<b>27.9</b>	<b>28.8</b>	<b>28.8</b>	<b>41.8</b>	<b>54.0</b>	<b>66.6</b>

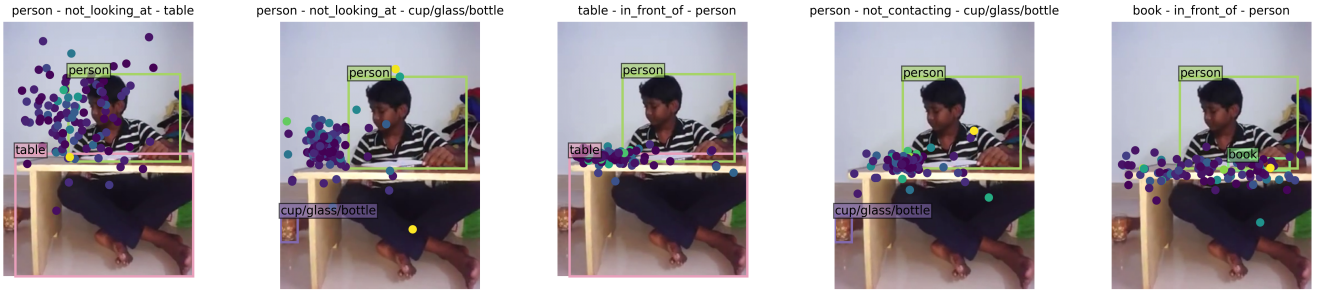


Figure 5. Visualization of sampling points of the Deformable Attention in the last Cross-Attention layer of FDSG’s entity decoder for the DSGG task. Brighter color indicates a larger attention weight associated with the sampling point. We also label the detected triplets and the bounding boxes.

## D.2. More DSGG and SGF Results

In Figs. 6-9, we present more DSGG and SGF results from FDSG. In particular, the results shown in Fig. 6 are contrasted with the qualitative results in Sec. 4.4 in our main paper. In this case, for SGF, the observed video fraction is  $\mathcal{F} = 0.5$ . In comparison, the Sec. 4.4 example has  $\mathcal{F} = 0.7$ , and in the last observed frame, the bottle on the left is clearly visible, and the person is also looking to the left, showing a clear intention to interact with the bottle.

However, when  $\mathcal{F} = 0.5$ , FDSG fails to detect the bottle due to partial occlusion in the last observed frame. In addition, the person is looking at the notebook and has not yet started the interaction with the bottle. Consequently, in SGF, our model does not predict any interaction between the person and the bottle. Instead, FDSG forecasts food / sandwich showing up in the center, again demonstrating that it has a comprehensive understanding of the scene and is capable of forecasting unseen actions.

Table 10. Comparison with state-of-the-art Scene Graph Anticipation methods on Grounded Action Genome Scenes (GAGS). Best and second best values are highlighted in **boldface** and underlined, respectively.

$\mathcal{F}$	Method	Recall@K (R@K) $\uparrow$						Mean Recall@K (mR@K) $\uparrow$					
		With Constraint			No Constraint			With Constraint			No Constraint		
		10	20	50	10	20	50	10	20	50	10	20	50
0.3	STTran++ [9, 33]	30.7	33.1	33.1	35.9	51.7	64.1	11.8	13.3	13.3	16.5	29.3	50.2
	DSG-DETR++ [11, 33]	25.7	28.2	28.2	36.1	50.7	64.0	11.1	12.8	12.8	19.7	32.0	51.1
	SceneSayerODE [33]	34.9	37.3	37.3	40.5	54.1	63.9	15.1	16.6	16.6	19.6	31.6	55.8
	SceneSayerSDE [33]	39.7	42.2	42.3	46.9	59.1	65.2	18.4	20.5	20.5	24.6	37.8	59.0
	Ours	<b>41.3</b>	<b>44.0</b>	<b>44.0</b>	<b>54.1</b>	<b>62.1</b>	<b>69.0</b>	<b>21.2</b>	<b>24.5</b>	<b>24.6</b>	<b>26.5</b>	<b>41.0</b>	<b>61.3</b>
0.5	STTran++ [9, 33]	35.6	38.1	38.1	40.3	58.4	72.2	13.4	15.2	15.2	17.8	32.5	53.7
	DSG-DETR++ [11, 33]	29.3	31.9	32.0	40.3	56.9	72.0	12.2	13.8	13.9	20.6	34.3	54.0
	SceneSayerODE [33]	40.7	43.4	43.4	47.0	62.2	72.4	17.4	19.2	19.3	22.8	35.2	60.2
	SceneSayerSDE [33]	45.0	47.7	47.7	52.5	66.4	73.5	20.7	23.0	23.1	26.6	40.8	63.8
	Ours	<b>49.1</b>	<b>52.6</b>	<b>52.6</b>	<b>56.4</b>	<b>70.2</b>	<b>75.1</b>	<b>24.5</b>	<b>27.4</b>	<b>27.4</b>	<b>29.5</b>	<b>43.7</b>	<b>67.0</b>
0.7	STTran++ [9, 33]	41.3	43.6	43.6	48.2	68.8	82.0	16.3	18.2	18.2	22.3	39.5	63.1
	DSG-DETR++ [11, 33]	33.9	36.3	36.3	48.0	66.7	81.9	14.2	15.9	15.9	24.5	41.1	63.4
	SceneSayerODE [33]	49.1	51.6	51.6	58.0	74.0	82.8	21.0	22.9	22.9	27.3	43.2	70.5
	SceneSayerSDE [33]	<u>52.0</u>	<u>54.5</u>	<u>54.5</u>	<u>61.8</u>	<u>76.7</u>	<u>83.4</u>	<u>24.1</u>	<u>26.5</u>	<u>26.5</u>	<u>31.9</u>	<u>48.0</u>	<u>74.2</u>
	Ours	<b>54.7</b>	<b>56.7</b>	<b>56.7</b>	<b>64.6</b>	<b>80.0</b>	<b>86.3</b>	<b>27.3</b>	<b>30.3</b>	<b>30.3</b>	<b>35.1</b>	<b>51.4</b>	<b>78.6</b>
0.9	STTran++ [9, 33]	46.0	47.7	47.7	60.2	81.5	92.3	19.6	21.4	21.4	29.6	49.1	76.4
	DSG-DETR++ [11, 33]	38.1	39.8	39.8	58.8	78.8	92.2	16.3	17.7	17.7	30.7	50.3	77.2
	SceneSayerODE [33]	58.1	59.8	59.8	72.6	86.7	93.2	25.0	26.4	26.4	35.0	51.7	80.2
	SceneSayerSDE [33]	<u>60.3</u>	<u>61.9</u>	<u>61.9</u>	<u>74.8</u>	<u>88.0</u>	<u>93.5</u>	<u>28.5</u>	<u>29.8</u>	<u>29.8</u>	<u>40.0</u>	<u>57.7</u>	<u>87.2</u>
	Ours	<b>63.6</b>	<b>65.0</b>	<b>65.0</b>	<b>77.0</b>	<b>91.0</b>	<b>96.5</b>	<b>31.3</b>	<b>33.3</b>	<b>33.4</b>	<b>44.5</b>	<b>60.2</b>	<b>90.8</b>

Table 11. Comparison with baseline methods on Action Genome for the Scene Graph Forecasting (SGF) task. Best values are highlighted in **boldface**.

$\mathcal{F}$	Method	Recall@K (R@K) $\uparrow$						Mean Recall@K (mR@K) $\uparrow$					
		With Constraint			No Constraint			With Constraint			No Constraint		
		10	20	50	10	20	50	10	20	50	10	20	50
0.3	SceneSayerODE+ [33]	0.7	0.9	0.9	0.7	1.0	1.3	0.4	0.5	0.5	0.5	0.8	1.4
	SceneSayerSDE+ [33]	2.1	2.6	2.8	3.0	4.0	4.5	1.1	1.4	1.6	1.3	2.0	3.5
	Ours	<b>9.2</b>	<b>11.4</b>	<b>13.1</b>	<b>10.2</b>	<b>13.1</b>	<b>16.2</b>	<b>7.6</b>	<b>9.7</b>	<b>11.3</b>	<b>9.2</b>	<b>14.2</b>	<b>18.5</b>
0.5	SceneSayerODE+ [33]	0.9	1.0	1.1	0.9	1.2	1.6	0.5	0.6	0.6	0.6	1.0	1.7
	SceneSayerSDE+ [33]	2.5	3.2	3.4	2.6	3.7	5.0	1.1	1.6	1.7	1.4	2.2	4.4
	Ours	<b>10.6</b>	<b>13.3</b>	<b>15.5</b>	<b>12.0</b>	<b>15.5</b>	<b>18.8</b>	<b>8.4</b>	<b>11.2</b>	<b>12.6</b>	<b>11.4</b>	<b>17.2</b>	<b>22.5</b>
0.7	SceneSayerODE+ [33]	1.3	1.5	1.5	1.3	1.7	2.2	0.7	0.8	0.8	0.9	1.4	2.3
	SceneSayerSDE+ [33]	2.9	3.5	3.8	3.0	4.1	5.5	1.5	2.0	2.2	1.7	2.9	5.1
	Ours	<b>13.0</b>	<b>15.6</b>	<b>17.8</b>	<b>14.3</b>	<b>18.4</b>	<b>21.5</b>	<b>9.9</b>	<b>12.8</b>	<b>14.1</b>	<b>12.4</b>	<b>18.1</b>	<b>23.1</b>
0.9	SceneSayerODE+ [33]	1.5	1.7	1.7	1.7	2.1	2.7	0.9	1.0	1.0	1.1	2.0	2.9
	SceneSayerSDE+ [33]	3.5	4.4	4.6	3.7	5.1	6.8	1.8	2.4	2.6	2.1	3.6	6.3
	Ours	<b>19.9</b>	<b>23.8</b>	<b>27.6</b>	<b>22.4</b>	<b>27.4</b>	<b>32.5</b>	<b>14.6</b>	<b>18.4</b>	<b>20.7</b>	<b>18.1</b>	<b>24.4</b>	<b>32.9</b>



Table 12. Ablation study of model components with Recall metrics. For Dynamic Scene Graph Generation (DSGG) and Scene Graph Forecasting (SGF) the task is SGDET, while for Scene Graph Anticipation (SGA) the task is AGS. For SGA and SGF, the observed fraction  $\mathcal{F} = 0.5$ . Notations for the model components: S - Static SG Module; T - Temporal Aggregation Module; TDM - Triplet Dynamics Model; LDM - Location Dynamics Model. Best values are highlighted in **boldface**.

Task	#	Model Component				Recall@K (R@K) $\uparrow$					
		S	T	TDM	LDM	With Constraint			No Constraint		
						10	20	50	10	20	50
DSGG	1	✓				33.4	41.0	48.1	35.2	45.0	54.0
	2	✓	✓			34.6	42.2	49.2	36.5	46.4	55.5
	3	✓	✓	✓		34.9	42.4	49.3	36.7	46.6	55.7
	4	✓		✓		33.4	41.0	48.1	35.3	45.1	54.2
	5	✓		✓	✓	33.3	40.8	47.9	35.2	45.0	53.8
	6	✓	✓	✓	✓	<b>35.3</b>	<b>42.9</b>	<b>49.8</b>	<b>37.2</b>	<b>47.4</b>	<b>56.4</b>
SGA	3	✓	✓	✓		28.1	36.5	45.8	29.7	39.9	<b>52.9</b>
	4	✓		✓		<b>28.4</b>	<b>36.8</b>	<b>46.3</b>	<b>30.6</b>	<b>40.7</b>	52.7
	5	✓		✓	✓	27.2	35.1	44.6	29.0	38.9	50.0
	6	✓	✓	✓	✓	28.2	36.5	45.5	29.8	40.1	52.0
SGF	5	✓		✓	✓	9.5	12.2	14.4	10.5	13.9	17.7
	6	✓	✓	✓	✓	<b>10.6</b>	<b>13.3</b>	<b>15.5</b>	<b>12.0</b>	<b>15.5</b>	<b>18.8</b>

Table 13. Ablation study of model components with Mean Recall metrics. DSGG and SGF are tested on SGDET and SGA is tested on AGS. For SGA and SGF, the observed fraction  $\mathcal{F} = 0.5$ . Best values are highlighted in **boldface**.

Task	#	Model Component				Mean Recall@K (mR@K) $\uparrow$					
		S	T	TE	LDM	With Constraint			No Constraint		
						10	20	50	10	20	50
DSGG	1	✓				19.7	25.8	30.9	24.5	38.2	52.0
	2	✓	✓			21.5	27.3	33.0	26.2	39.3	50.8
	3	✓	✓	✓		21.0	27.2	32.0	26.0	39.5	52.5
	4	✓		✓		19.7	25.8	30.9	24.8	38.3	52.2
	5	✓		✓	✓	19.7	25.8	30.9	24.6	38.2	51.9
	6	✓	✓	✓	✓	<b>22.2</b>	<b>27.8</b>	<b>33.0</b>	<b>27.8</b>	<b>42.0</b>	<b>54.1</b>
SGA	3	✓	✓	✓		14.5	21.5	26.9	17.7	29.9	43.1
	4	✓		✓		16.6	21.8	27.2	19.5	31.7	44.5
	5	✓		✓	✓	16.2	21.9	28.3	20.8	31.6	44.4
	6	✓	✓	✓	✓	<b>18.1</b>	<b>23.5</b>	<b>27.5</b>	<b>23.2</b>	<b>34.3</b>	<b>45.8</b>
SGF	5	✓		✓	✓	6.6	10.1	11.0	8.5	13.6	19.0
	6	✓	✓	✓	✓	<b>8.4</b>	<b>11.2</b>	<b>12.6</b>	<b>11.4</b>	<b>17.2</b>	<b>22.5</b>

In Figs. 7-9, for SGF, the observed video fraction is  $\mathcal{F} = 0.5$ . In Fig. 7, the video shows a man cleaning his room with a broom. FDSG is able to forecast the movement of the broom. In Fig. 8, the video shows a man leaving his laptop to fetch some food. FDSG forecasts that the man would interact with the box in front of him, instead of the food that is farther away. In Fig. 9, the video shows a woman taking off her shoes. FDSG forecasts that the woman would interact with her clothes, which is very close to the precise action of removing shoes.

Table 14. Comparison between different temporal aggregation strategies. (a) aggregating forecasts before observations; (b) aggregating both information in a single cross-attention layer. Best values are highlighted in **boldface**.

Task	Method	Recall (R)						Mean Recall (mR)					
		With Constraint			No Constraint			With Constraint			No Constraint		
		10	20	50	10	20	50	10	20	50	10	20	50
DSGG	(a)	35.0	42.4	49.3	37.0	46.9	55.9	21.0	27.1	31.9	26.0	39.8	53.0
	(b)	34.7	42.0	49.0	36.7	46.5	55.5	21.1	27.3	32.0	26.3	39.8	51.8
	Ours	<b>35.3</b>	<b>42.9</b>	<b>49.8</b>	<b>37.2</b>	<b>47.2</b>	<b>56.5</b>	<b>22.2</b>	<b>27.8</b>	<b>33.0</b>	<b>27.8</b>	<b>42.0</b>	<b>54.1</b>
SGA $\mathcal{F} = 0.5$	(a)	25.9	32.6	39.8	27.5	36.7	48.7	11.3	14.6	17.7	13.7	22.3	34.6
	(b)	28.1	35.7	43.4	28.8	38.6	50.7	13.3	17.3	20.8	16.8	26.1	38.7
	Ours	<b>28.3</b>	<b>36.5</b>	<b>45.3</b>	<b>30.1</b>	<b>40.4</b>	<b>52.2</b>	<b>18.1</b>	<b>23.5</b>	<b>27.5</b>	<b>23.2</b>	<b>34.3</b>	<b>45.8</b>
SGF $\mathcal{F} = 0.5$	(a)	7.0	8.3	9.7	7.8	10.1	12.8	4.8	5.9	6.9	5.8	9.6	13.8
	(b)	8.6	10.5	12.1	9.4	12.0	14.8	5.9	7.5	8.6	7.6	11.7	15.9
	Ours	<b>10.6</b>	<b>13.3</b>	<b>15.5</b>	<b>12.0</b>	<b>15.5</b>	<b>18.8</b>	<b>8.4</b>	<b>11.2</b>	<b>12.6</b>	<b>11.4</b>	<b>17.2</b>	<b>22.5</b>

Table 15. Object detection recall and average precision for SGF with different observation fraction  $\mathcal{F}$ .

Observed Fraction $\mathcal{F}$	Object Detection Recall R@20						AP (IoU $\geq 0.5$ )		
	SGA (IoU $\geq 0$ )			SGF (IoU $\geq 0.5$ )					
	Baseline	Oracle	Ours	Baseline	Oracle	Ours	Baseline	Oracle	Ours
0.3	77.00	77.05	81.57	37.07	39.23	40.67	9.1	14.0	10.8
0.5	80.11	82.75	83.36	40.33	44.01	43.85	10.5	16.3	12.1
0.7	84.44	89.76	87.38	45.67	51.27	47.87	13.3	23.7	16.7
0.9	86.99	96.01	91.89	55.25	64.95	58.51	18.7	37.5	22.2

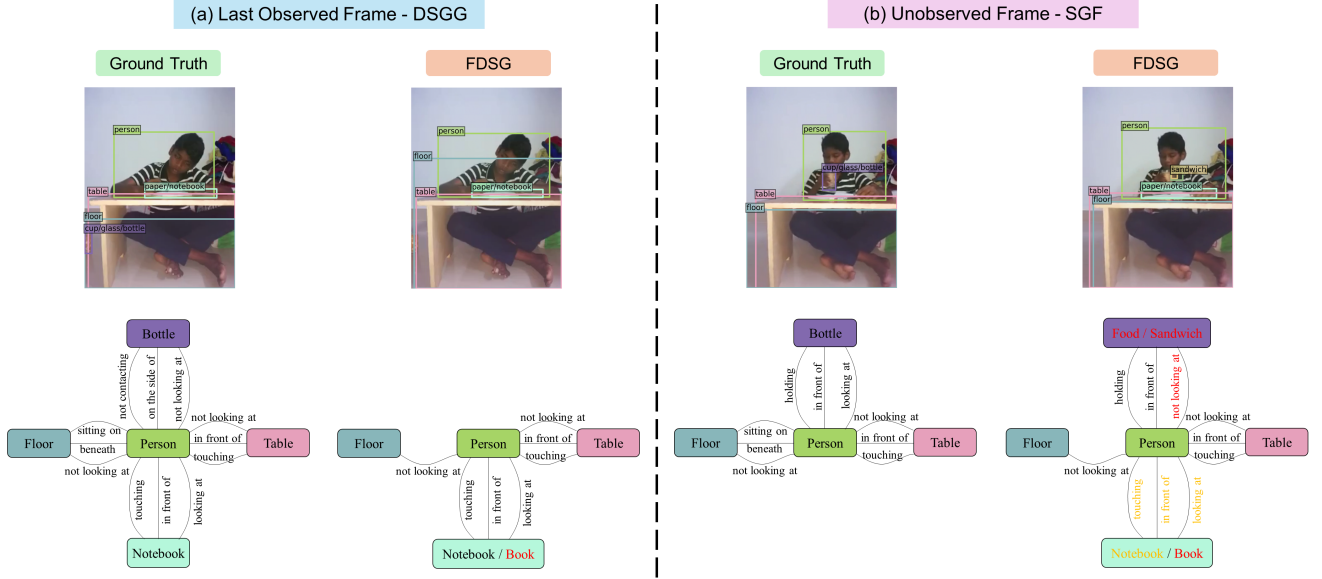


Figure 6. Visualization of Dynamic Scene Graph Generation (DSGG) and Scene Graph Forecasting (SGF) outputs from our FDSG. The first row shows frames and ground truth / predicted entity bounding boxes, while the second row shows corresponding scene graphs. In the scene graphs, incorrect predicates are highlighted with text in red, while entities / predicates with missing labels in the ground truth are highlighted in orange. For (a) observed frames, we provide our DSGG results and compare them with the ground truth. For (b) unobserved frames, we contrast our SGF results to the ground truth.

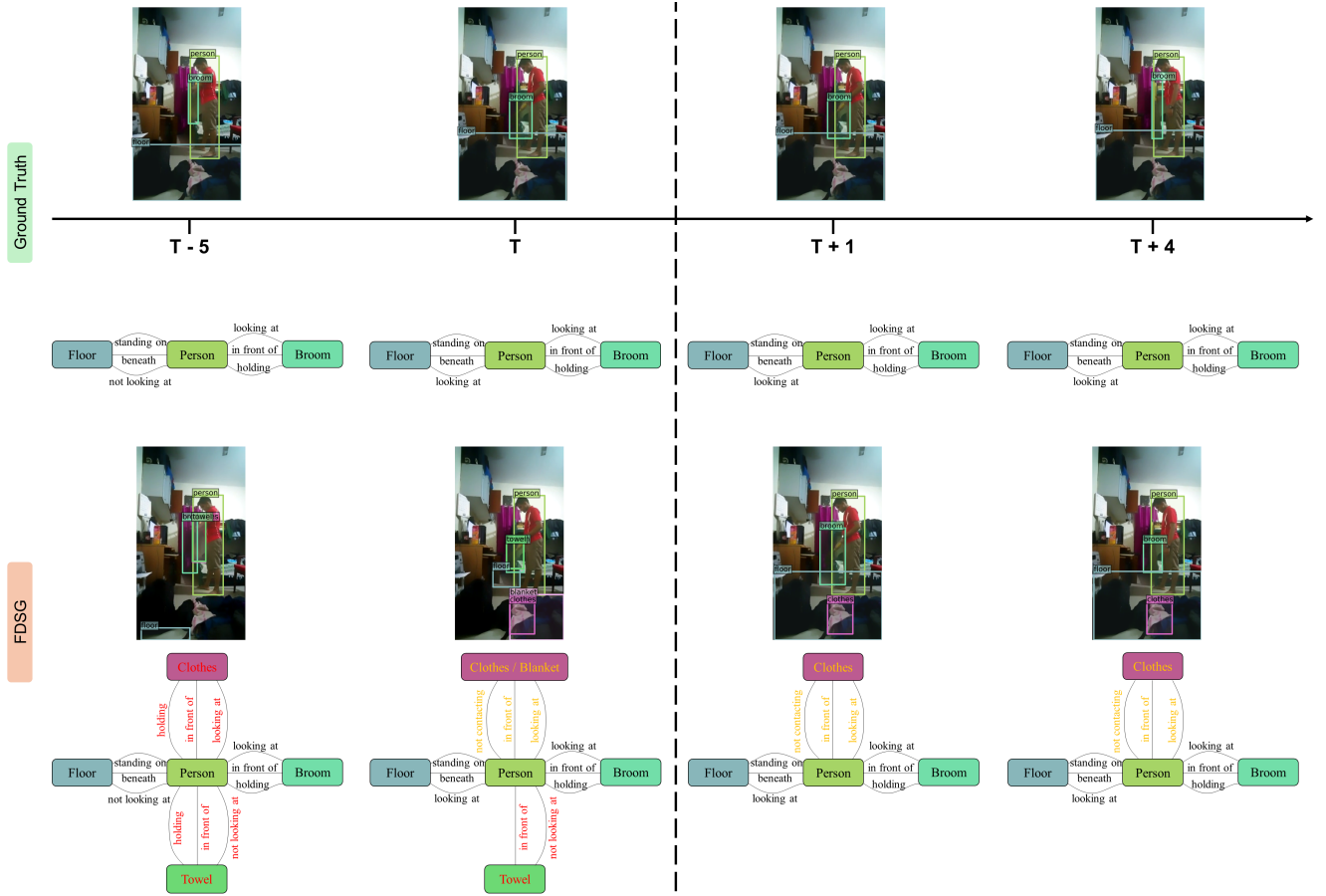


Figure 7. Visualization of Dynamic Scene Graph Generation (DSGG) and Scene Graph Forecasting (SGF) outputs from our FDSG. The first two rows show frames with ground truth entity bounding boxes and ground truth scene graphs, while the last two rows show generated scene graphs from DSGG or SGF. In the scene graphs, incorrect predicates are highlighted with text in red, while entities / predicates with missing labels in the ground truth are highlighted in orange.

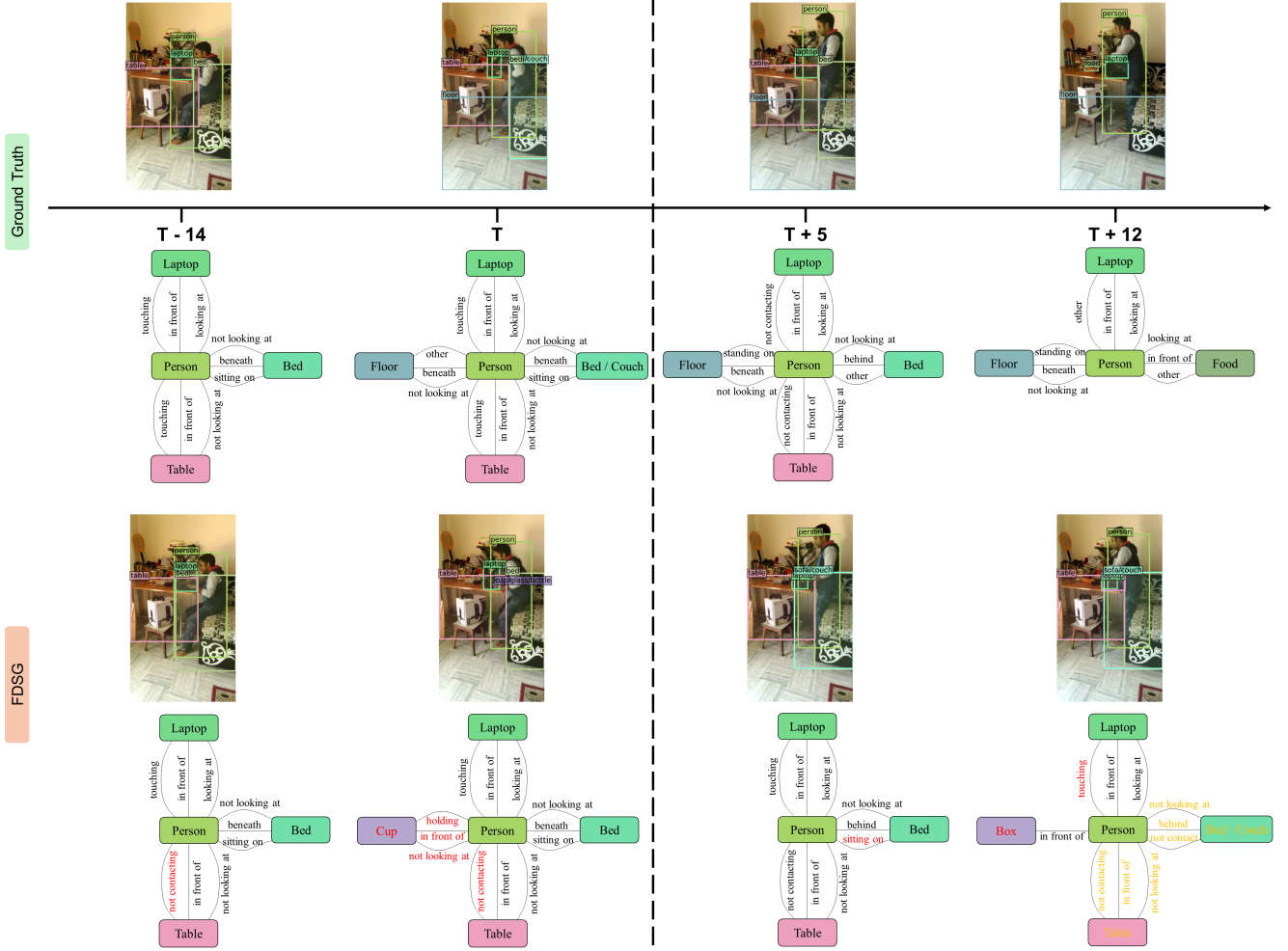


Figure 8. Visualization of Dynamic Scene Graph Generation (DSGG) and Scene Graph Forecasting (SGF) outputs from our FDSG. The first two rows show frames with ground truth entity bounding boxes and ground truth scene graphs, while the last two rows show generated scene graphs from DSGG or SGF. In the scene graphs, incorrect predicates are highlighted with text in red, while entities / predicates with missing labels in the ground truth are highlighted in orange.



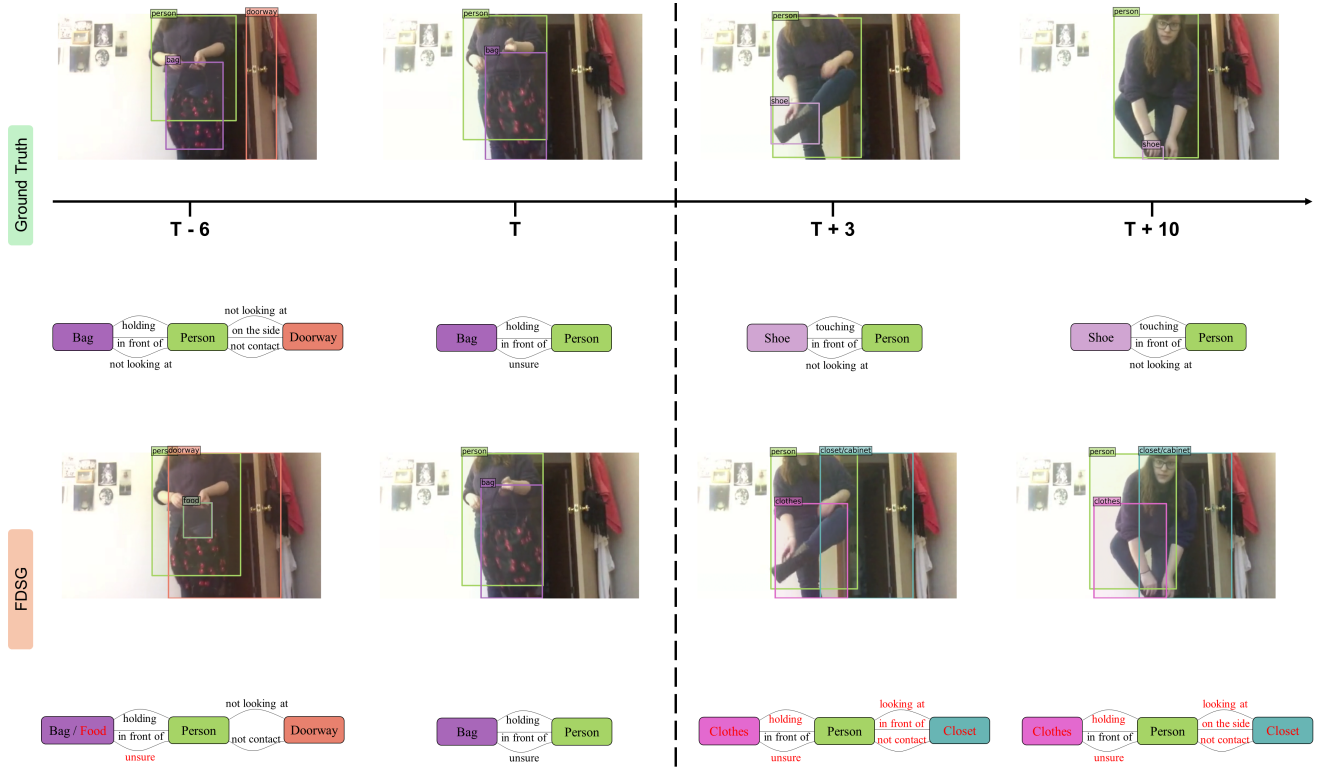


Figure 9. Visualization of Dynamic Scene Graph Generation (DSGG) and Scene Graph Forecasting (SGF) outputs from our FDSG. The first two rows show frames with ground truth entity bounding boxes and ground truth scene graphs, while the last two rows show generated scene graphs from DSGG or SGF. In the scene graphs, incorrect predicates are highlighted with text in red, while entities / predicates with missing labels in the ground truth are highlighted in orange.